GEOMORPHIC MAPPING AND GROUND-PENETRATING RADAR SURVEY OF THE WESTERN SEGMENT OF THE AGUA BLANCA FAULT, BAJA CALIFORNIA, MEXICO

by

SARAH RUTH MADSEN

Bachelor of Science, 2006
University of Texas at Dallas
Richardson, Texas

Submitted to the Graduate Faculty of
The College of Science and Engineering
Texas Christian University
in partial fulfillment of the requirements
for the degree of

MASTER OF SCIENCE

August 2009

ACKNOWLEDGEMENTS

I would first like to gratefully thank the Dean and Associate Deans of the College of Science and Engineering at Texas Christian University for agreeing to finance my master's degree, without which I could not have afforded to attend such a prestigious institution. Special thanks and eternal gratitude to my direct advisor, Dr. Helge Alsleben, for his insight, encouragement, mentorship and patience – I was definitely not the only one who spent many stressful hours working toward the success of this project. A special thanks to the ranchers and families that allowed us on their property to gather data for this study. I am indebted to my other committee members, Dr. Arthur Busbey and Dr. Richard Hanson, for their precious time and knowledge. A tip of my hat to the other professors, staff and colleagues in the Department of Geology, specifically Dr. Nowell Donovan, Dr. John Breyer, Mrs. Terri Mabe, and Mr. Dave McCleery; many mentorships and friendships have been forged and will be cherished. And, of course, I am beholden to my tolerant husband, Nathan, and my wonderful family and friends, especially Rachael Monroe and Jen Mele, for enduring the mania.

TABLE OF CONTENTS

LIST OF FIGURES

LIST OF FIGURES (CONTINUED)

LIST OF FIGURES (CONTINUED)

LIST OF TABLES

Chapter 1: Introduction

1.1 Statement of Problem

The role of the Agua Blanca fault zone within the North American plate boundary system is poorly understood. The fundamental question is whether the fault is currently active and simply late in its earthquake cycle, as suggested by Rockwell *et al.* (1993) and Dixon *et al.* (2002), or whether the fault has become inactive. In order to address that fundamental question, several other questions emerge. For example, if the fault has recently been active, how is the fault expressed at the surface? What is the character of the fault in the subsurface? The goal of this thesis is to examine the western segment of the Agua Blanca fault system and to resolve these questions as part of a detailed surface and near-surface assessment of the entire fault system.

1.2 Purpose of Study

The west-northwest- to east-southeast-trending Agua Blanca fault zone, which is associated with the Pacific-North American transform plate boundary, is commonly interpreted as an active, dextral strike-slip fault that traverses Baja California, Mexico, near latitude 31º30'N (Allen *et al*., 1960) (Figure 1). The onshore portion of the main fault is approximately 120 km in length and is divided into three right-stepping, approximately 40-km long segments (Rockwell *et al.,* 1993). The eastern fault segment extends from Valle de Trinidad to Valle Agua Blanca, and the central portion runs from Valle Agua Blanca through the southeastern portion of Valle Santo Tomas (Figure 1 and 2). The westernmost segment bounds the southeastern edge of Valle Santo Tomas before it splits into a southern fault (Santo Tomas fault) and a northern fault, located

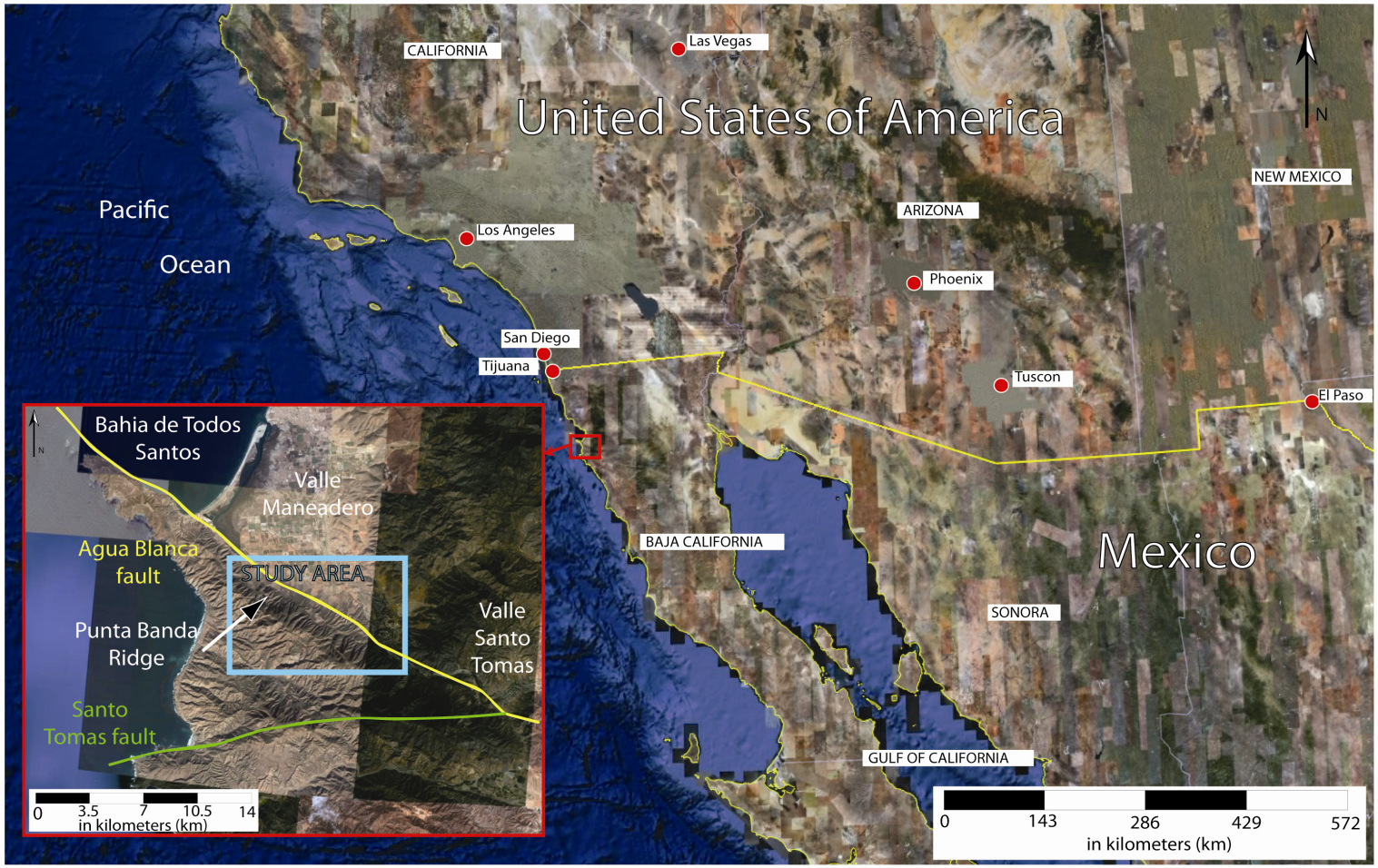

Figure 1. Location map of the Agua Blanca fault system within the North American continent, modified from Google Earth Images. Inset identifies geographic landforms. The blue box represents the study area for this project.

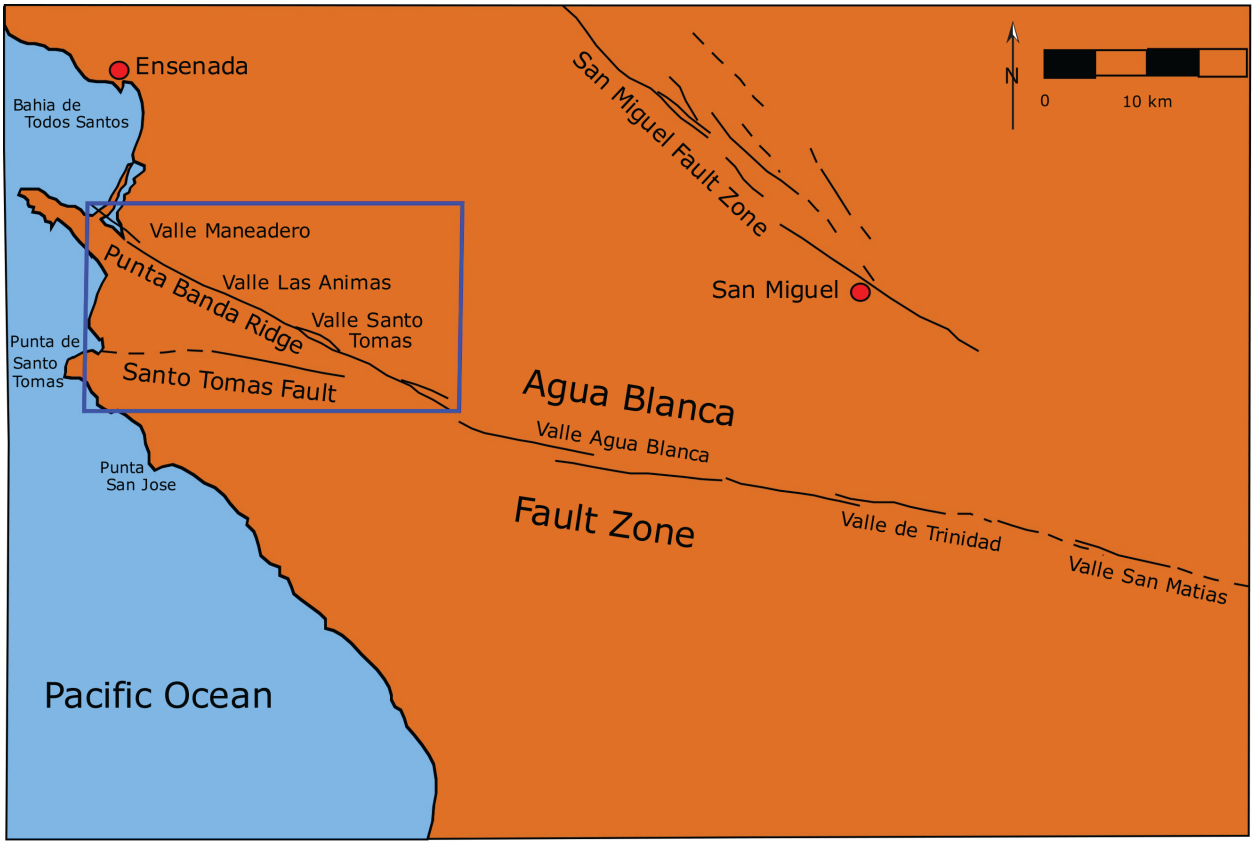

Figure 2. Location map of Agua Blanca and San Miguel faults. Blue box indicates current and planned study sites along the western segment of the Agua Blanca fault. Modified from Rockwell *et al*. (1993).

along the northern edge of Punta Banda Ridge. The northern fault, which is interpreted as the main fault trace, continues offshore into the Bahia de Todo Santos (Rockwell *et al.*, 1993) (Figure1), and is thought to link with faults offshore (Legg *et al.*, 1991; Rockwell *et al*., 1993).

Reasons for studying the Agua Blanca fault zone are four-fold. Firstly, the transform plate boundary, which includes the San Andreas system of California, extends into northwestern Mexico, where faults are less well studied and understood. Studies south of the border are limited (Allen *et al.*, 1960; Gastil *et al.*, 1975, 1981; Schug, 1987; Legg *et al.*, 1991; Rockwell *et al.*,1993; Dixon *et al.*, 2002), while a considerable amount of literature has been published on the California portion of this plate boundary (e.g., Atwater, 1970; Dickinson and Snyder, 1979; Wilson, 1988; Wallace, 1990; Dickinson, 1996; Atwater and Stock, 1998; Wesnousky, 2005). In order to understand the dynamics of the entire plate boundary system, fault studies south of the border must be completed.

Secondly, the only geologic study of the Agua Blanca fault zone was completed prior to the general acceptance of the theory of plate tectonics (Allen *et al.,* 1960). Subsequent investigations of the Agua Blanca fault zone attempted to study fault strands using trenches (Hatch, 1987; Schug, 1987; Hilinski, 1988; Rockwell *et al.,* 1993), placed the fault zone into a tectonic context without further detailed study (Suarez-Vidal *et al.,* 1991), or used geodetic data to estimate fault slip rates (Dixon *et al.,* 2002). Speculation about recent activity on the fault has culminated in the fundamental question whether the fault is currently active and simply late in its earthquake cycle or whether the fault has become inactive. The lack of seismicity along this fault within the last 200 years could indicate a partial transfer of displacement to the

nearby San Miguel fault (Figure 2), a young fault that is better aligned with the northwest-southeast trend of the North American plate boundary system (Dixon *et al.*, 2002). To address whether the fault is active or not, the present study was designed to document potential surface and near-surface evidence for recent activity along the western segment of the Agua Blanca fault system.

Thirdly, the question of how the fault is expressed at the surface has only been partly addressed. In 1987, Thomas Rockwell and his student, David Schug used aerial photographs to complete geomorphic mapping on a section of the western segment of the Agua Blanca fault system (Schug, 1987). They categorized the Quaternary alluvial deposits and noted a variety of offset surface features (Schug, 1987). More recent technology, such as Google Earth, provides detailed satellite images that clearly show probable fault splays and other geomorphic features, such as pressure ridges, that require field verification. A new interpretation, including the incorporation of geomorphic field maps and an updated list of observed characteristics of the Agua Blanca fault zone, such as offset stream channels and locations of fault breccia, gouge and scarps, will supplement our understanding of this part of the fault system.

Fourth, trenches completed by Schug (1987) are the only study of the western segment of the fault that investigates the shallow subsurface. Schug (1987) concluded that the fault system is expressed in the subsurface as a single vertical trace surrounded by minor infilled fractures. Although trenching studies can provide tangible evidence of fault locations, the dimensions of the trench limit the data to an isolated point within the system. Subsurface imaging technology, such as ground-penetrating radar, has matured within the last 20 years (Baker *et al.*, 2007). This cost-effective and

expeditious surveying method supplies reliable information on geologic features within the near-surface, allowing data to be collected at many points within a field area.

In order to begin addressing these issues, the following objectives were completed for my project. Firstly, I completed detailed geologic maps within three study areas along the westernmost segment of the Agua Blanca fault (Figure 3). Special attention was paid to geomorphic features, such as triangular facets, that indicate fault location, and features that suggest recent movement along the fault, such as deflected stream channels. Fault traces were located within each field area and evidence for recent fault activity was recorded. Secondly, GPR surveys were completed within the field areas, which provided near-surface images of the main fault trace and fault splays as well as stratigraphic contacts between alluvial packages.

1.3 Introduction to Geomorphic Features associated with Active Tectonism

Within active tectonic regions, geomorphic features, such as escarpments, triangular facets, fault scarps, offset stream channels, pressure ridges and shutter ridges are common surface expressions of fault traces (Bull, 2007). Escarpments are produced when elevated terrain with steep cliffs is adjacent to low-lying terrain. These are large-scale geomorphic features that can be associated with faulting within an active tectonic region. For example, movement along a strike-slip fault can bring a portion of topographically higher terrain adjacent to a region of topographically lower terrain. Escarpments are not common in regions experiencing reverse faulting; however, the downward movement of the hanging wall of a normal fault will often expose the fault surface as a scarp face. Erosion of the scarp face produces characteristic triangular

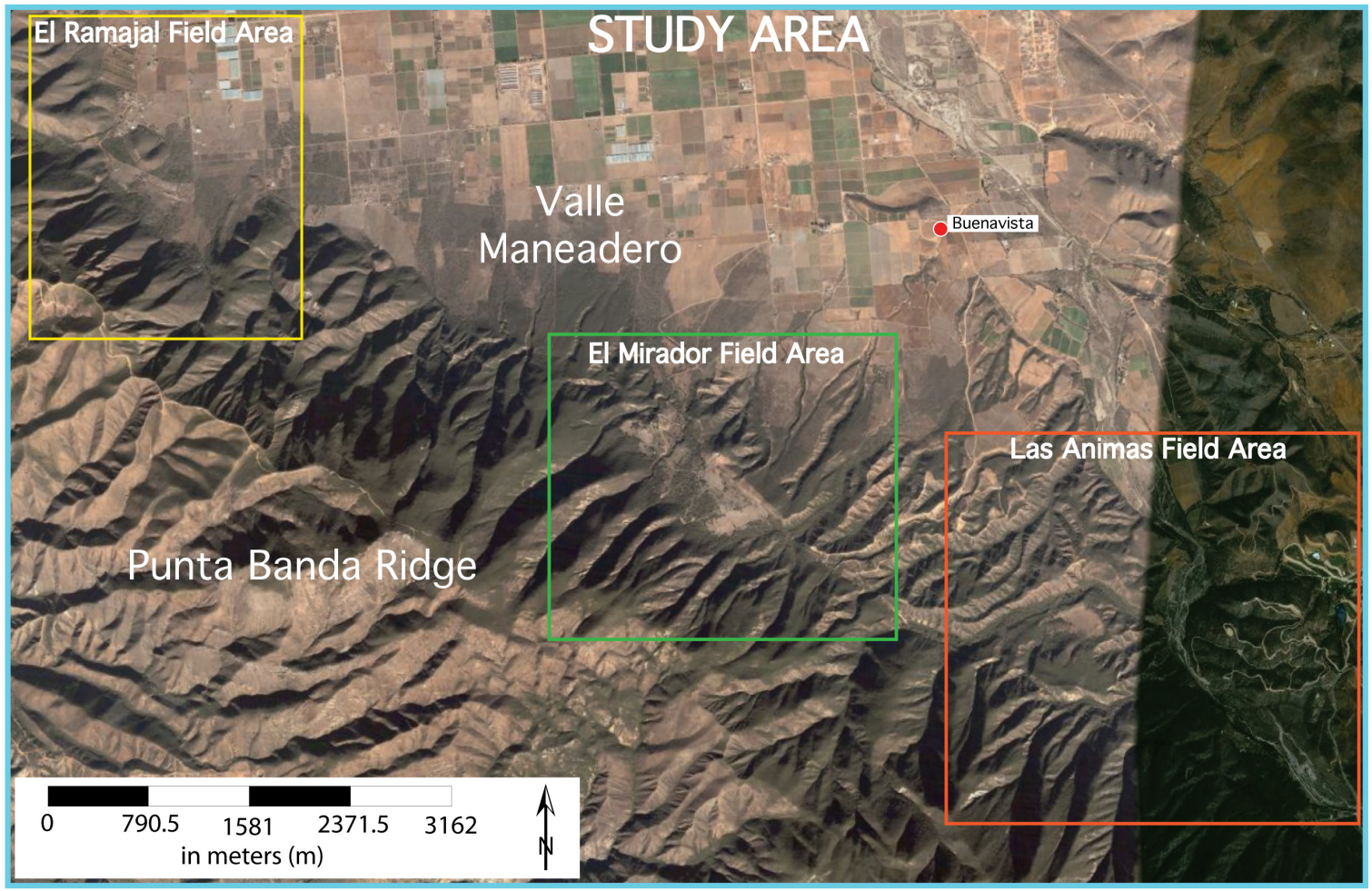

Figure 3. Location map of field areas for this study, modified from Google Earth Images.

facets. Development of triangular facets indicates vertical motion along the fault trace, which is common even if the fault is dominantly characterized by strike-slip movement. Fault scarps are small-scale escarpments and can be the surface expression of a fault trace, either exposing a cliff of resistant bedrock or a pile of sediments due to slope failure within weaker units. Offset stream channels are active stream channels that have been bisected by an active fault and are common within strike-slip faulting regimes. As movement occurs along the fault, stream channels bend to compensate, and as time progresses, this bend often becomes a sharp, 90° deflection in the flow of the channel. Pressure ridges are created by convergent directions of movement along strike-slip fault step-overs, or by small bends in a single strike-slip fault strand. The result of transpression is an isolated, circular topographic high that often diverts the sediment transport around the structure. Shutter ridges also impede sediment transport from the escarpment into the low-lying valley; however, these structures are often long, linear portions of the escarpment itself that have been shifted along the fault. These features can create accommodation space for increased sediment deposition between them and the escarpment until the shutter ridge is breached.

1.4 Introduction to Ground-Penetrating Radar

Ground-penetrating radar (GPR) surveys provide relatively fast and noninvasive imaging of the shallow subsurface. The basic system incorporates four pieces of equipment connected by fiber optic cables: a transmitter and receiver (each attached to an antenna), and a control unit and a digital video logger (DVL) (Figure 4). The transmitter emits high-frequency (1-1000MHz) electromagnetic (EM) pulses directed

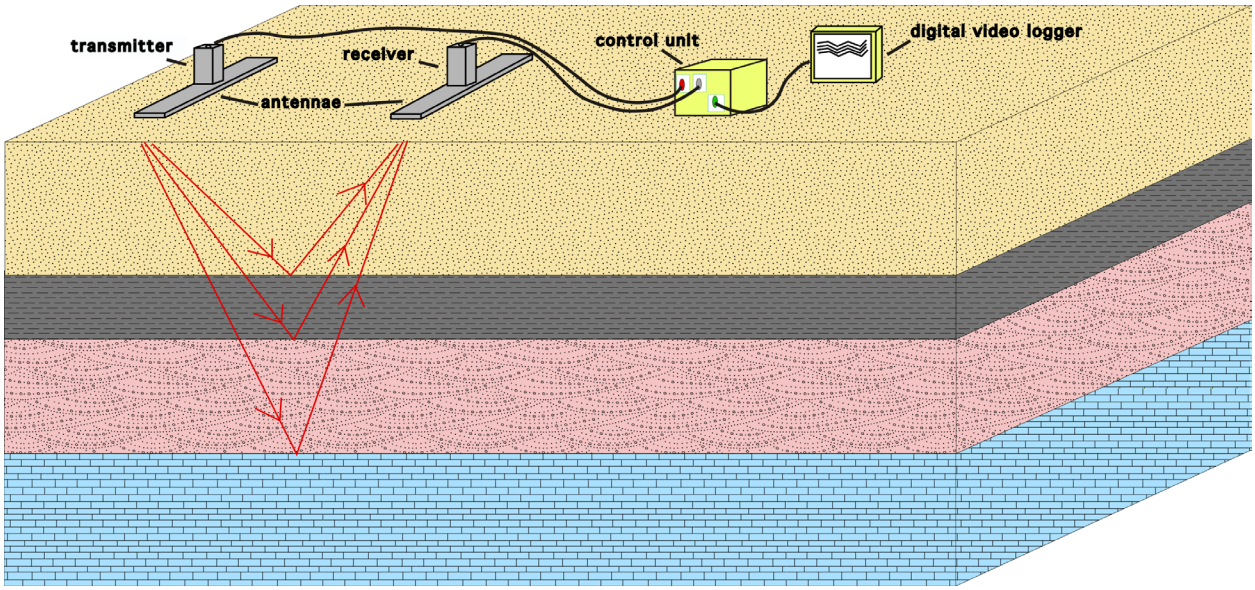

Figure 4. Basic ground-penetrating radar equipment and function. An EM pulse is emitted from the transmitter through the antenna and into the Earth (shown as down-going red arrows). The signals reflect, refract and diffract off the contacts between geologic units with differing physical properties (the blue, pink, grey and beige units) and are redirected toward the surface (shown as the up-going red arrows). The signals are collected by the receiver at the surface and stored in the control unit. The digital video logger is attached to the system for real-time display of data points as they are collected. Based on information from Baker *et al*. (2007).

into the Earth by the attached antenna placed on the surface (Yetton and Nobes, 1998; Baker *et al.*, 2007). As the EM waves propagate, they reflect, diffract and refract off stratigraphic and structural boundaries and portions of the signals return to the surface. Returning signals are captured at the surface by the antenna attached to the receiver, which records the time interval elapsed between transmitting and receiving signals (Yetton and Nobes, 1998). The recorded data is transferred to the control unit where it is organized for real-time display on the DVL, a liquid-crystal display interface attached to the system for input of survey parameters and manipulation of survey results.

Reflection, diffraction and refraction of the EM waves are due to changes in propagation velocity at stratigraphic and structural interfaces (Baker *et al.*, 2007). Propagation velocity of the EM waves is directly controlled by relative dielectric permittivity, which measures the capacity of a material to store and then permit the passage of EM energy when under the influence of an electric field (Cai *et al.*, 1996; Baker *et al.*, 2007). An increase in relative dielectric permittivity results in a decrease in propagation velocity (Cai *et al.*, 1996; Burger *et al.*, 2006; Baker *et al.*, 2007). In general, the relative dielectric permittivity of all Earth materials is greater than the permittivity of air (Table 1); therefore the propagation velocity of an EM wave in all Earth materials will be less than the EM propagation velocity in air (0.3 m/ns) (Baker *et al.*, 2007).

Of great importance to GPR surveys are signal resolution, depth of penetration and the factors that control both of these values. Signal resolution and depth of penetration are inversely related; the greater the depth of penetration, the lower the resolution of the signal. Spherical spreading and signal attenuation control both of these factors (Burger *et al.*, 2006). Spherical spreading results in a decrease in the strength of

Material	Conductivity (mS/m)[a]	Relative Permittivity	Radar velocity (m/ns)[b]
Salt water	3000	81-88	0.01
Fresh water	0.5	80	0.033
Wet sand	0.1-1	20-30	0.06
Clay	2-1000	5-40	0.06-0.17
Shale	1-100	5-15	0.09
Concrete	0.01-10	6	0.09
Limestone	0.5-2	4-8	0.12
Granite	0.01-1	4-6	0.13
Dry sand	0.01	3-10	0.15
Ice	0.01	3-4	0.16
Air	0	1	0.3

[a] metersiemens per meter
[b] meters per nanosecond

Table 1. List of Earth materials with associated conductivities, relative permittivities, and radar velocities (after Burger *et al.,* 2006).

the signal in relation to the distance from the source; the spreading extends out in all directions (Burger *et al.*, 2006). Signal attenuation is a reduction in the intensity of an EM wave due to scattering of the signal out of the path of the receiver and absorption of the EM wave by the geologic material (Burger *et al*., 2006). Attenuation is regulated by the magnetic permeability and the electrical conductivity of the medium (Baker *et al.*, 2007). Magnetic permeability is the capacity of a material to become magnetized when influenced by an EM field and electrical conductivity is the ability of the material to conduct electrical currents (Burger *et al.,* 2006). As both of these properties increase, EM energy is attenuated, resulting in loss of the signal (Burger *et al.*, 2006). High water tables, buried pipes and layers of clays or evaporites have elevated values for both of these parameters and can negatively affect EM energy.

Several different survey types can be used depending on ease of movement in the terrain and available length of fiber optic cable (Figure 5 A and B). A common mid-point survey is used for calibration in each new location within a study area. The curve resulting from this survey type provides an optimum propagation velocity for reflection surveying based on the rock type. The antennae are stepped away from a central location and data are either gathered continuously or the pulse is sent by way of a time-delayed sequence when the antennae are static. Reflection surveys are another survey type, where data can be gathered continuously or at static points. During the survey, the antennae are separated by a fixed distance and moved in the same direction. Stacked signals can be viewed on the DVL. The data require post-processing to reduce noise and boost the amplitude of the signals for aid in interpretation.

5A

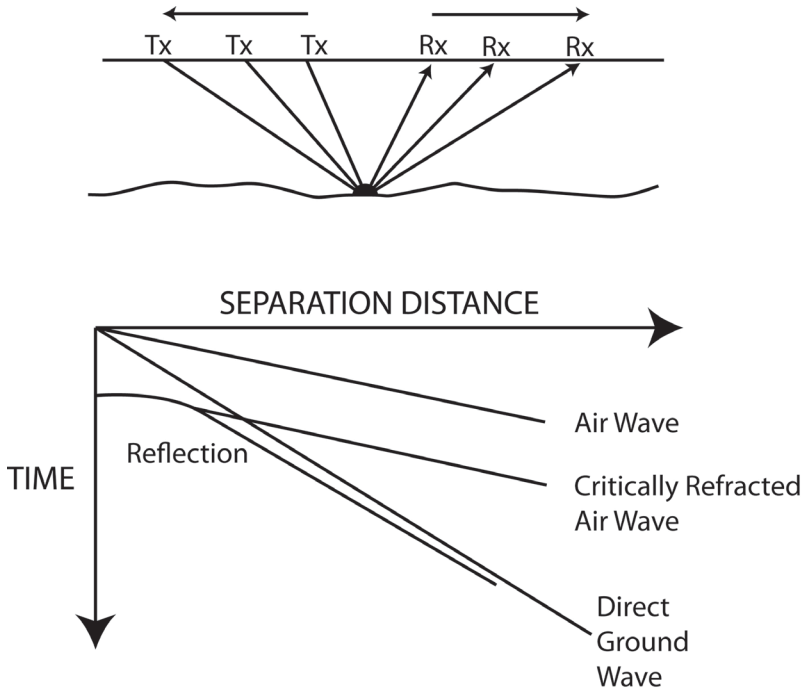

5B

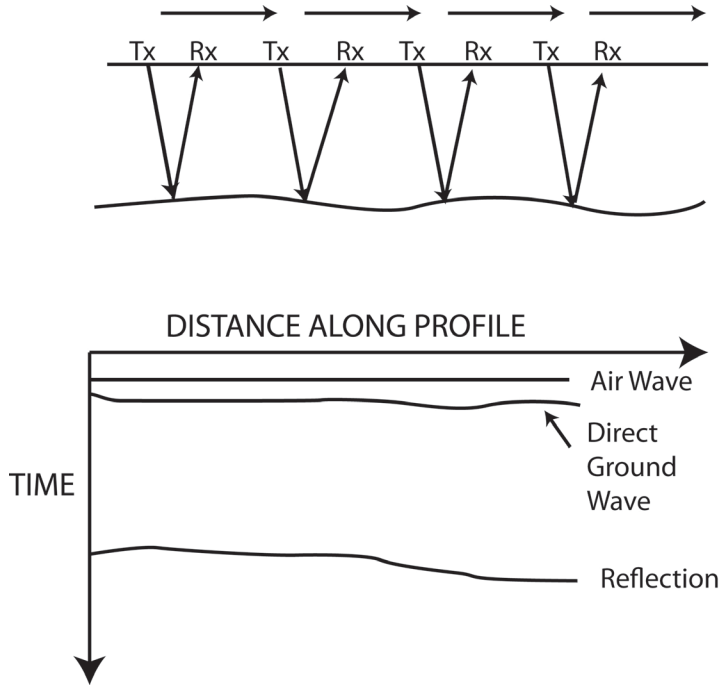

Figure 5 A and B. Methods of survey using ground-penetrating radar. (A) common mid-point survey (CMP); (B) reflection survey. Modified from Baker *et al.* (2007).

GPR has been used successfully to image faults in plate boundary systems. Cai *et al.* (1996) completed GPR surveys of the San Andreas and Hayward faults in northern California. They chose specific locations near previous trenching sites in order to compare the two types of data. The GPR surveys produced high-quality data that allowed correlation between the GPR and trenching results. Yetton and Nobes (1998) imaged the Alpine fault in New Zealand using GPR equipment. The fault is a right-lateral strike-slip fault that accommodates deformation as the Pacific and Australian plates slide past each other. These workers were able to image up to 20 m beneath the surface and identify offset features across a series of fault splays (Figure 6). Similarly, Slater and Niemi (2003) were able to image the Dead Sea transform fault that separates the African and Arabian plates. Although issues arose with signal attenuation from high salt concentration and reworked sediments, they were able to identify fault contacts in their surveys.

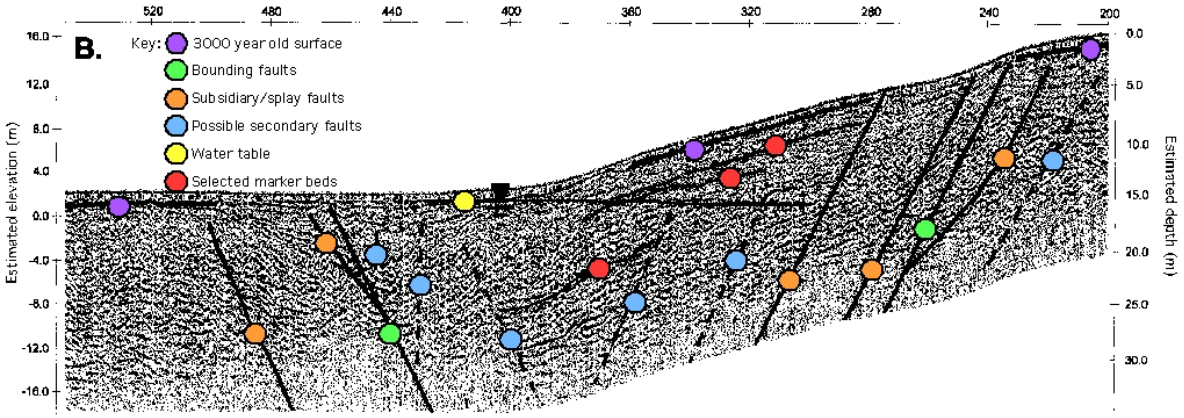

Figure 6. Ground-penetrating radar survey of the Alpine Fault, New Zealand. The colors define the type of reflector and both scales are in meters. From Yetton and Nobes (1998).

Chapter 2: Geologic Background

2.1 Tectonic Evolution of the North American Plate Boundary System

The Agua Blanca fault is thought to be an inherited structure (Gastil *et al.*, 1981; Wetmore *et al.*, 2002, 2003). Gastil *et al*. (1981) postulated that the Agua Blanca fault is a reactivated Cretaceous structure and interpreted the fault as a former oceanic left-lateral trench-trench transform fault involved in the Cretaceous subduction of the Farallon plate beneath the North American plate. This idea was further explored by Suarez-Vidal *et al.* (1991), who postulated that the structure was reactivated as a right-lateral fault to partially accommodate the onset of the opening of the Gulf of California. Dickinson (1996), however, argued against this interpretation, claiming that faults entering the head of the gulf take up the transmitted lateral slip of the rift system. Building on studies by Gastil *et al.* (1981), Wetmore *et al.* (2002, 2003) postulated that the fault zone originally acted as a sinistral transpressional continuation of the Late Cretaceous suture (Main Martir fault) that juxtaposes the mid-Cretaceous Alisitos island arc volcanics with the North American continent (Wetmore *et al.*, 2002). The resulting zone of weakness in the crust is thought to have been reactivated during the Cenozoic as part of the San Andreas fault system to aid in accommodation of plate boundary deformation as the Pacific and North American plates interacted (Atwater, 1970).

Reactivation of the Agua Blanca fault zone would have occurred as a result of interaction between the Pacific, North American, and Farallon plates (Atwater, 1970). In the early Cenozoic, subduction rates at the North American plate boundary (Figure 7) were 7-10 cm/yr (Atwater, 1970). Simultaneously, segmented spreading ridges of the East Pacific Rise, which separated the Farallon and Pacific plates, created new oceanic

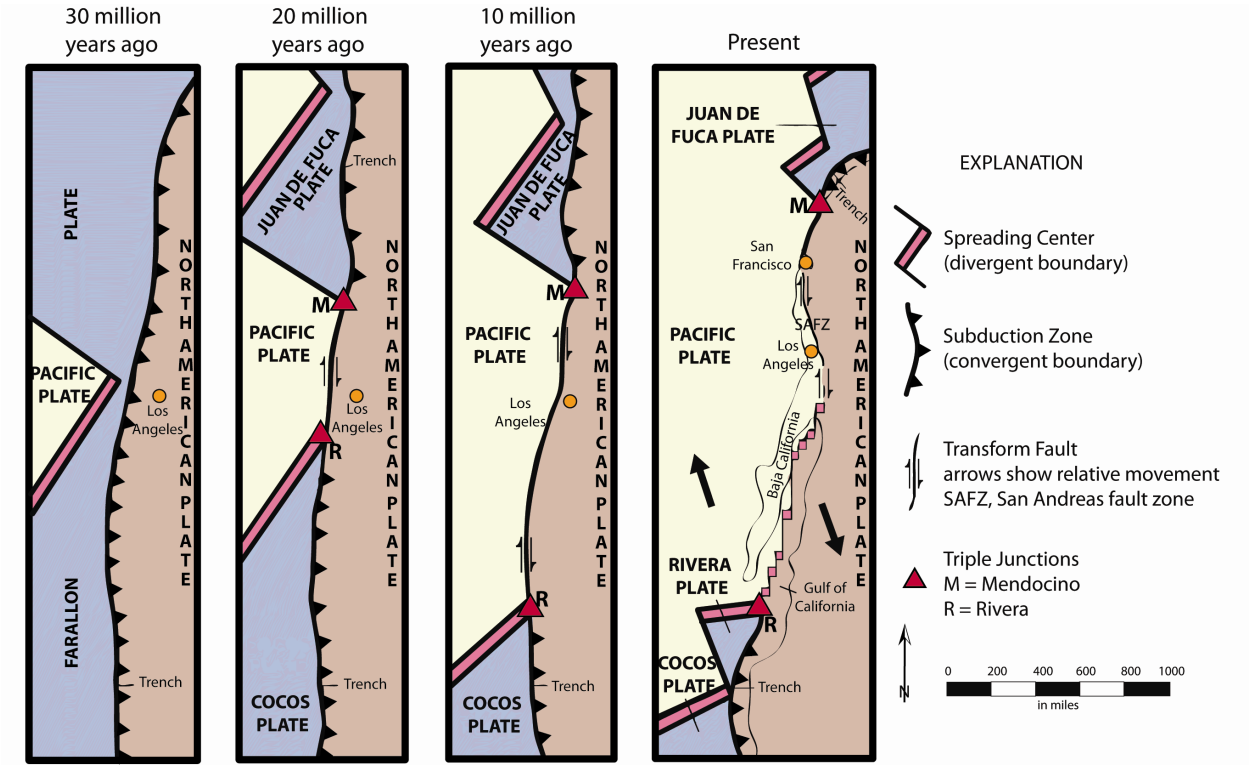

Figure 7. Evolution of Pacific – North American plate transform boundary system, From Irwin (1990).

crust at an estimated rate of 5 cm/yr (Atwater, 1970). This difference in rates resulted in slow migration of these ridges toward the trench (Atwater, 1970). When the Pacific plate came into contact with the North American plate between 28 and 25 Ma, an unstable quadruple junction formed that converted into two stable triple junctions (Figure 7): the Mendocino triple junction in the north and the Rivera triple junction in the south (McKenzie and Morgan, 1969; Stock and Molnar, 1988; Atwater, 1989; Irwin, 1990). With continued subduction of the remnants of the Farallon plate, these triple junctions migrated away from each other along a continuously growing transform fault system (Irwin, 1990) (Figure 7).

Initially, plate boundary deformation was accommodated mostly within the continental margin, called the California continental borderland, prior to affecting the continental interior as movement along the San Andreas fault (Figure 8) (Atwater, 1989; Dickinson, 1996). Accommodation of nearly all Pacific and North American plate motion along the malleable continental margin was likely caused by addition of young, hot oceanic crust to the accretionary wedge (Atwater, 1970). After a cooling period of 5 to 7 m.y., the borderland became rigid and lost the capacity to take up most of the plate boundary deformation within the continental margin (Atwater, 1970). As deformation moved inland, faults associated with the San Andreas fault system, such as the San Gregorio–Hosgri fault, the Santa Cruz–San Isidro fault, and faults in the western Transverse Ranges, began to accommodate portions of the total deformation before initiation of the San Andreas fault proper between 18 and 12 Ma (Atwater, 1970; Dickinson, 1996).

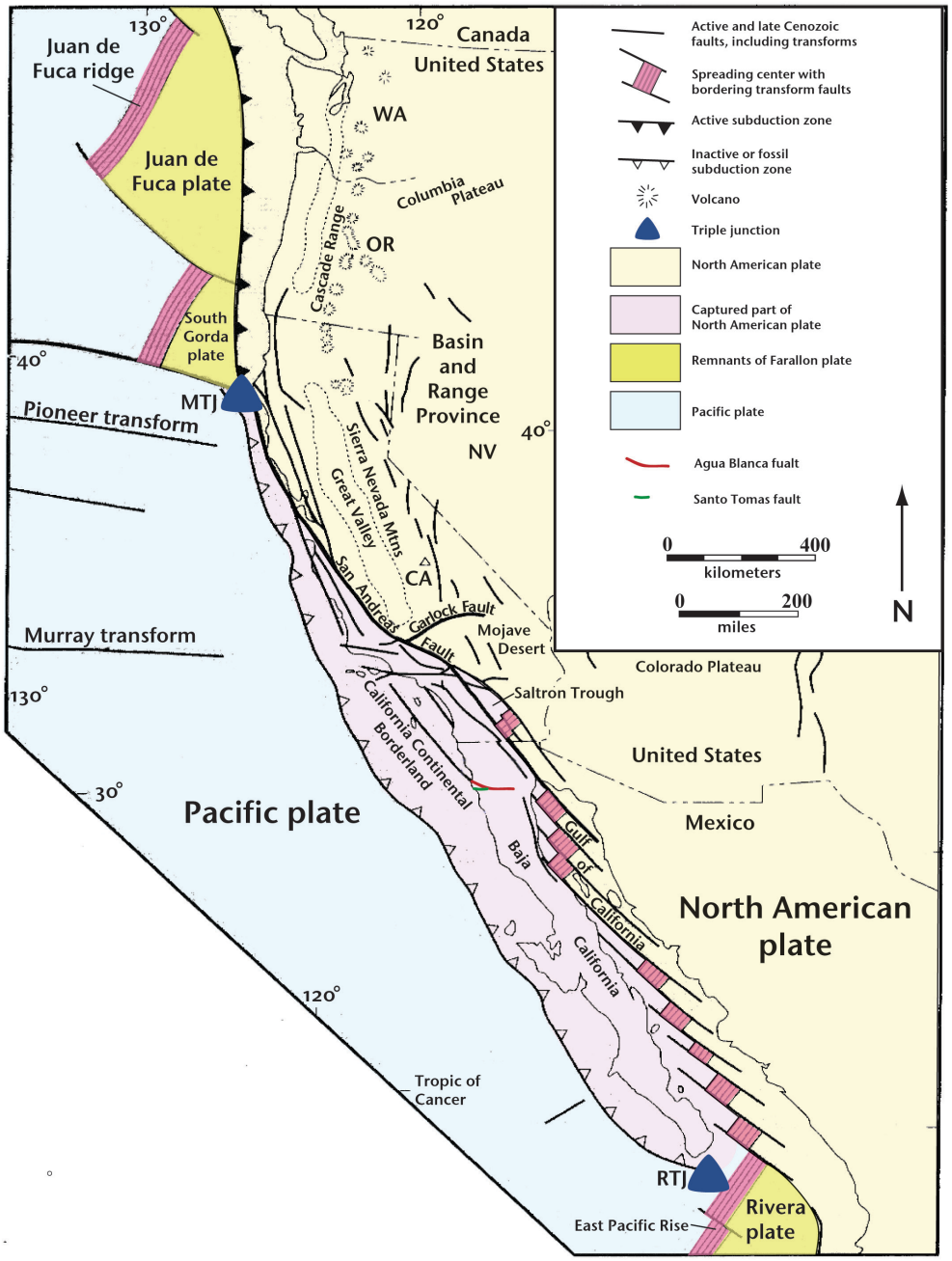

Figure 8. Map of current plate tectonic setting of Western North America. MTJ = Mendocino triple junction, RTJ = Rivera triple junction. Outline of plates and states from Hatcher (1995). Tectonic units from Irwin (1990).

Today, transform motion within the current plate boundary configuration (Figure 8) is divided mostly between the San Andreas fault system and the Walker Lane fault system (Figure 9), which includes the Eastern California shear zone (Wesnousky, 2005). Some of the deformation is possibly taken up by the Basin and Range province (Wesnousky, 2005). The sum of the maximum right-lateral displacement rates for faults within the San Andreas fault system subtracted from the total relative motion between the Pacific and North American plates determines the percentage of deformation accommodated by the San Andreas fault system (Thatcher, 1990). The average rate of movement on all of the faults within the San Andreas fault system is 33-37 mm/yr, and the relative plate motion of the Pacific-North American plate system is 49 ± 3 mm/yr (Thatcher, 1990). Therefore the San Andreas fault system currently accommodates the majority (70-80%) of the relative plate motion of the Pacific–North American plate system (Thatcher, 1990), emphasizing the importance of understanding all of the individual components of this system.

2.2 Previous Work on the Agua Blanca Fault System

Allen *et al.* (1960) provided the first geologic overview of the Agua Blanca fault zone, incorporating information from earlier publications on the geology of northern Baja California by Bose and Wittich (1913), Santillan and Barrera (1930), Floras (1931) and Woodford and Harris (1938). Allen *et al.* (1960) described the fault zone as an active right-lateral strike-slip fault with subsidiary splays that trend and behave similarly. Those workers selected Agua Blanca Valley (Valle de Agua Blanca, Figure 2) as the type locality for the stratigraphic and structural definition of this fault system. Typical features

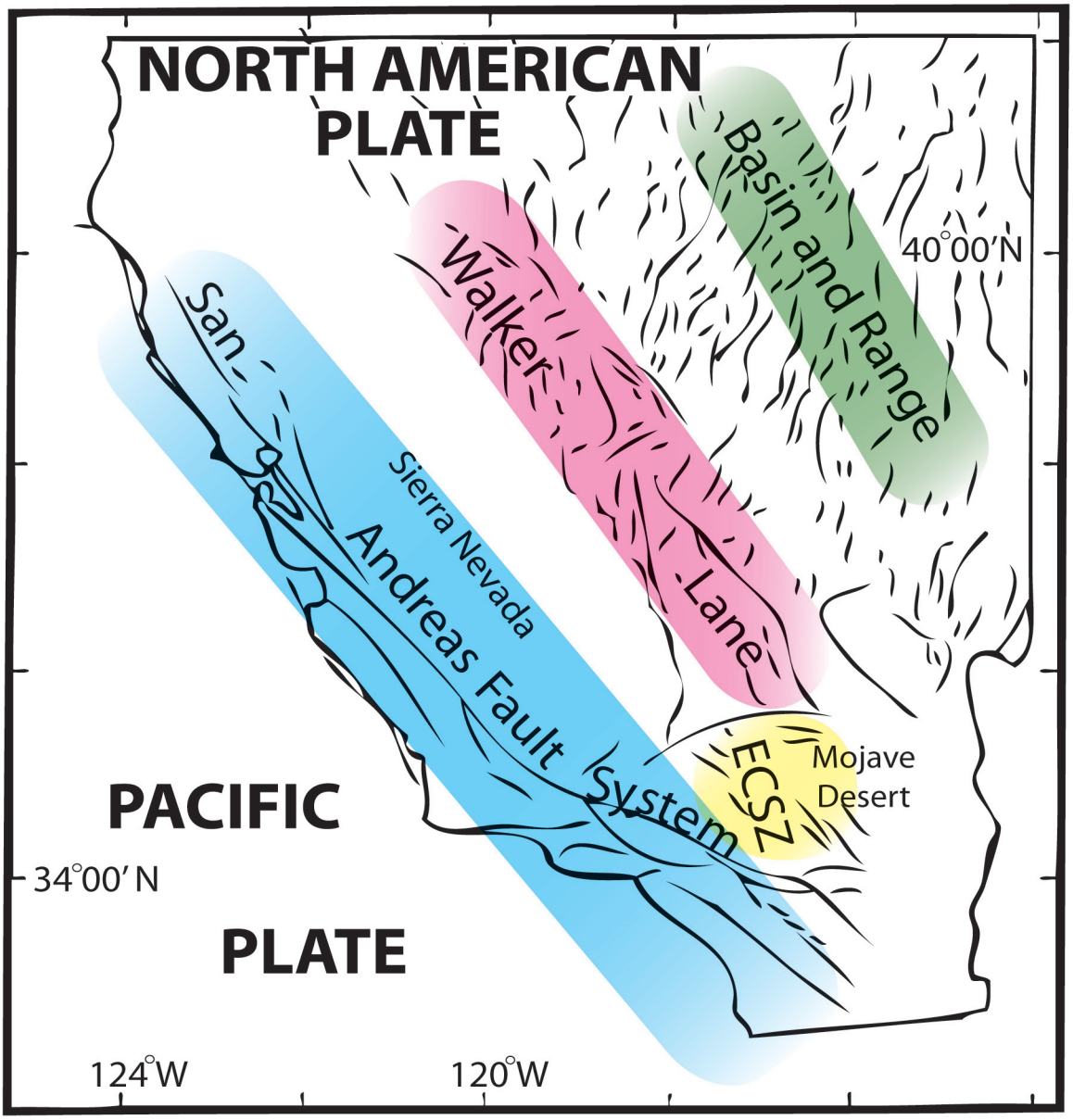

Figure 9. Location map of faults that accommodate most of the transform motion of the Pacific – North American transform boundary system. ECSZ = Eastern California shear zone. Map outline from Wesnousky (2005).

within this valley include recent scarps, offset streams, shutter ridges, fault sags, saddles, side-hill ridges and fault-controlled valleys (Allen *et al.,* 1960). Furthermore, the same workers used offset geomorphic features to estimate a range of displacement across the main fault between 4.8 and 22.5 km.

Following this earlier work, Hatch (1987), Hilinski (1988) and Schug (1987) completed thesis projects along segments of the Agua Blanca fault using trenching studies, aerial photos and limited field mapping. Hatch (1987) worked on the central segment while Hilinski (1988) studied the eastern segment. Schug (1987) focused on the westernmost Punta Banda segment, providing a basic framework for the current project. Rockwell *et al.* (1993) summarized these results and described the basic nature of the main Agua Blanca fault as three right-stepping fault segments that continue offshore. The detailed network of offshore extensions was previously described by Legg *et al.* (1991). Rockwell *et al.* (1993) were able to infer Holocene displacement of 40-60 m. Using limited age constraints, a range of slip-rates between 4 and 10 mm/yr with an average of 6 mm/yr was calculated for the type locality in Agua Blanca Valley (Rockwell *et al.,* 1993).

Two earthquake recurrence intervals were calculated along the Agua Blanca fault. Using radiocarbon ages, slip-rate estimates and assumptions based on the segmentation of the fault (Schug, 1987), 40-km-long surface ruptures roughly equal to the length of each of the three segments should produce strong earthquakes with moment magnitudes between 6.8 and 7.0. An average displacement of 0.5-1 m per earthquake should accompany earthquakes of these magnitudes and, upon incorporation of the average slip rates of 4-6 mm/yr for the Agua Blanca fault, the calculated earthquake recurrence interval is 90-250 years. A second recurrence interval

is based on available radiocarbon data from marine terraces that are offset 20-25 m along Punta Banda Ridge (Schug, 1987). Assuming the same average displacement of 0.5-1 m per earthquake, 20-50 earthquakes are required to produce the necessary offset. An earthquake recurrence interval of 100-375 years is inferred from the minimum (2500 years) and maximum (7500 years) age range for the terraces (Rockwell *et al.,* 1993).

Using geodetic data measured between 1993 and 1998 and earthquake data from the United States Geological Survey, Dixon *et al.* (2002) created virtual models to compare slip rates along the main Agua Blanca fault and the San Miguel fault (Figure 2) by accounting for rheological responses of the crust to the current regional stress regime. The available data for the main Agua Blanca fault suggested that the fault is active, but locked in the upper crust. The fault is likely accumulating strain to be released in a future earthquake with a moment magnitude between 6.1 and 7.0 (Dixon *et al.*, 2002).

2.3 Geology of the Study Area

The western segment of the Agua Blanca fault is characterized by a prominent west-northwest-trending mountain range termed Punta Banda Ridge. Two units, the Alisitos and El Rosario Formations, comprise the bedrock in this area. The northern portion of Punta Banda Ridge is adjacent to a low-lying coastal valley, Valle Maneadero. The valley as well as portions of the escarpment is overlain by Quaternary alluvial deposits.

The main bedrock unit within the study area is the mid-Cretaceous Alisitos Formation. Several petrologic studies of the Alisitos Formation have been completed

(Allison, 1955; Suarez-Vidal, 1987), showing that it consists of sedimentary and volcanic rocks including tuffaceous siltstones, limestones, sandstones, and volcanic breccias (Allison, 1955). The mid-Cretaceous age of the Alisitos Formation is constrained by a variety of well-preserved fossils (Allison, 1955) and limited geochronologic data (Johnson *et al.*, 1999). The environment of deposition is thought to be mostly marine, with marine fossils and pillow basalts as evidence, although some local depocenters near volcanic edifices were subaerially exposed (Fackler-Adams and Busby, 1998). Volcanic compositions range from andesite to basalt (Fackler-Adams and Busby, 1998).

The other bedrock unit in the area is the Upper Cretaceous El Rosario Formation, which unconformably overlies the Alisitos Formation. Sandstone and conglomerate dominate, although fossil-bearing limestone and shale are locally present (Lescinsky *et al.*, 1991). The age is constrained through bryozoans fossils and detrital zircons (Kimbrough *et al.*, 2001). The El Rosario Formation represents Upper Cretaceous forearc deposits (Lescinsky *et al.*, 1991).

The Quaternary alluvial deposits within the study area range in age from the Late Pleistocene (850 ka) to Recent and consist of angular, coarse gravel and sand derived from the Alisitos Formation (Schug, 1987). These sediments form alluvial fans, fluvial terraces and channel deposits (Schug, 1987). All of the Quaternary units mapped for this project are gravel dominated alluvial fan deposits and the gravel alluvial fan facies classification by Ekes and Friele (2003) was used to identify and define the facies within the mapped Quaternary units.

Chapter 3: Methods and Results

3.1 Field Areas

Initial reconnaissance mapping was completed along Punta Banda Ridge within Valle Maneadero and into Valle Santo Tomas (Figures 1 and 2). Certain areas were inaccessible or eliminated from the study due to gated private property, rough terrain, or poor exposure.

Three specific field areas were identified for detailed mapping (Figure 3). El Ramajal Field Area (FA1) is located along the westernmost portion of the Agua Blanca fault system, adjacent to the western terminus of Punta Banda Ridge near the Pacific Ocean. Most of the field work in this 13 km^2 area was completed along the mountain front that constitutes the southern boundary of Valle Maneadero. El Mirador Field Area (FA2) is a 9 km^2 region along the mountain front approximately 2 km east of FA1 along the fault zone. Las Animas Field Area (FA3) is also 9 km^2 and is approximately 0.5 km east of FA2 along the mountain front. This field area is located near a steep-walled stream channel that leads into Valle Las Animas between Valle Maneadero and Valle Santo Tomas. Most of the area within FA3 was located in steep and unstable topography.

3.2 Geomorphic Mapping

Geomorphic mapping at a scale of ~1:10,000 was carried out to accomplish two important objectives. The first objective was locating features suggestive of recent activity along the fault zone, such as deflected stream channels. The second objective was documentation of the fault trace by mapping and describing the local bedrock, recent alluvial deposits and identifying zones of fault breccia and gouge along the fault.

One field map was completed within each field area. Due to the 20 m contour interval of the topographic maps, geomorphic features smaller than 10 m were below the resolution of the mapping project.

3.2.1 Geomorphic Features and Faults

The main Agua Blanca fault is easily recognized in all three field areas. Evidence for the location of the main fault exists in the form of fault breccias and fault gouge. The main fault mostly cuts Cretaceous volcanic and volcaniclastic rocks related to the Alisitos arc. In the field areas, these volcanic units consist of plagioclase-rich volcanic rocks with light to medium gray matrices. Although the various lithologies were noted, good outcrops were scarce throughout the field areas and thicknesses of units or contact relationships between various units could not be properly established. Fracture patterns, however, were described and structural measurements were taken where possible. In addition to recognizing the main fault and various Alisitos arc–related volcanic units, certain geomorphic features, such as deflected stream channels and triangular facets were documented in all three field areas. Below I describe all the field areas in some detail, starting with the westernmost location (FA1) and then moving eastward to FA2 and FA3.

3.2.1.1 Field Area 1

A geologic map of FA1 is presented in Figure 10. FA1 is located along the northern edge of the Punta Banda Ridge southeast of the Punta Banda estuary in the vicinity of Rancho El Ramajal. In addition to the main northwest-southeast-trending

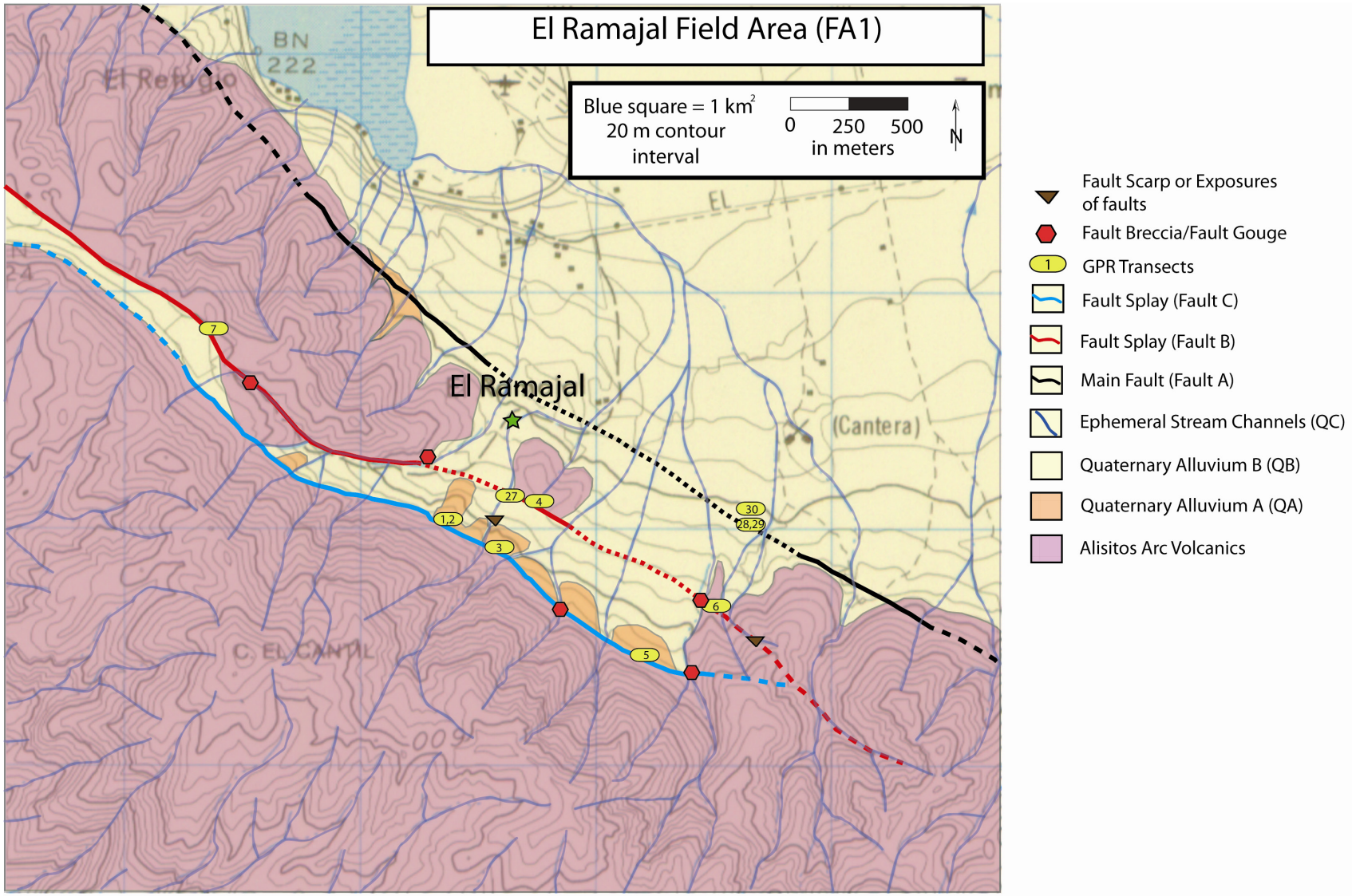

Figure 10. Field map of Field Area 1. Reference point is Rancho El Ramajal indicated by the green star. Fault rocks, fault exposures and locations of GPR surveys are indicated as well.

Agua Blanca fault (Fault A), two subsidiary, subparallel fault strands (Faults B and C) were identified to the south of the main fault (Figure 10).

Rocks within the zone of deformation of a fault, such as fault breccia and gouge, are found in various locations (Figure 10), and exposures exist where the fault cuts the volcanic bedrock in the field area. Interestingly, these fault-rock exposures are recognized only along the subsidiary fault splays (Faults B and C), whereas similar exposures along the main fault strand (Fault A) are not recognized in FA1. The best exposures of fault breccia along Fault B are at the northwestern end of the field area, where the breccia is bright orange with a tan to orange matrix and contains angular fragments ranging in size from a few millimeters to a few centimeters (Figure 11). Exposures of fault breccia along Fault C at the southeastern edge of the field area are characterized by very light-colored matrix and clasts (Figure 12). The bedrock in the area consists of volcanic rock dominated by plagioclase phenocrysts and lithic fragments, with the latter ranging from a few millimeters to one centimeter in size. Where the bedrock is affected by one of the faults, the original bedrock characteristics are almost obliterated. The rocks within the fault zones are crushed and have changed color. These color changes are the result of fluids flowing along the fault zones. However, small angular fragments within the fault breccias resemble the volcanic rocks that are exposed within several meters of the fault zones.

Although fault rock exposures are limited and the faults are partially covered by Quaternary alluvium, geomorphic evidence exists for the locations of the faults. Triangular facets are poorly developed in the bedrock along the mountain front south of the main fault trace (Fault A), and there are no facets associated with Fault B. South of

Figure 11. Fault breccia in volcanic rock along Fault B south of El Ramajal. Clasts are tan to orange volcanic fragments surrounded by orange matrix. Compass for scale.

Figure 12. Fault breccia in volcanic rock near eastern edge of FA1. Clasts range in size from a few millimeters to a few centimeters.

Fault C, however, facets are well-developed (Figure 13). In addition, several stream channels are deflected in a dextral sense across Fault C (Figure 14), although deflections were not obvious in small channels crossing Faults A or B. The isolated, roughly circular exposure of volcanic bedrock (Figure 13) located southeast of Ranch El Rajamal is either a small pressure ridge or represents the remnants of a breached shutter ridge. In the case of the former possibility, the pressure ridge would have formed along the small bend in Fault B to the northwest and has since been translated along the fault to its current position. Further evidence for relatively recent fault activity in the area is provided by the presence of an outcrop of Fault B cutting Quaternary alluvium near the southeastern end of the fault (Figure 15). A possible fault scarp was also found affecting Quaternary alluvial deposits roughly 500 m south of Rancho El Ramajal (Figure 16). This scarp is 15-20 meters high, but not directly located along Fault C. Whether this small scarp represents another fault splay or recent mass wasting could not be established due to the limited exposure and human alteration of the landscape.

Fracture orientations were measured mostly in bedrock to the south of Fault C (Figure 10). Bedrock exposures are generally within a few meters of the fault trace, although in a few cases exposures had to be followed into the stream channels several tens of meters from the fault. Stereonets were constructed using the fracture data (Figure 17 and 18). These limited data show two main trends, suggesting the existence of systematic fracture sets in the area, although several nonsystematic fractures exist. Figure 17 shows moderately to steeply dipping (average ~68°), north-northeast-south-southwest-trending fractures. A second set of fractures is shown in Figure 18. Here, fractures are also moderately to steeply dipping, but trend in an east-northeast-west-southwest orientation. The two fracture trends may represent a conjugate set.

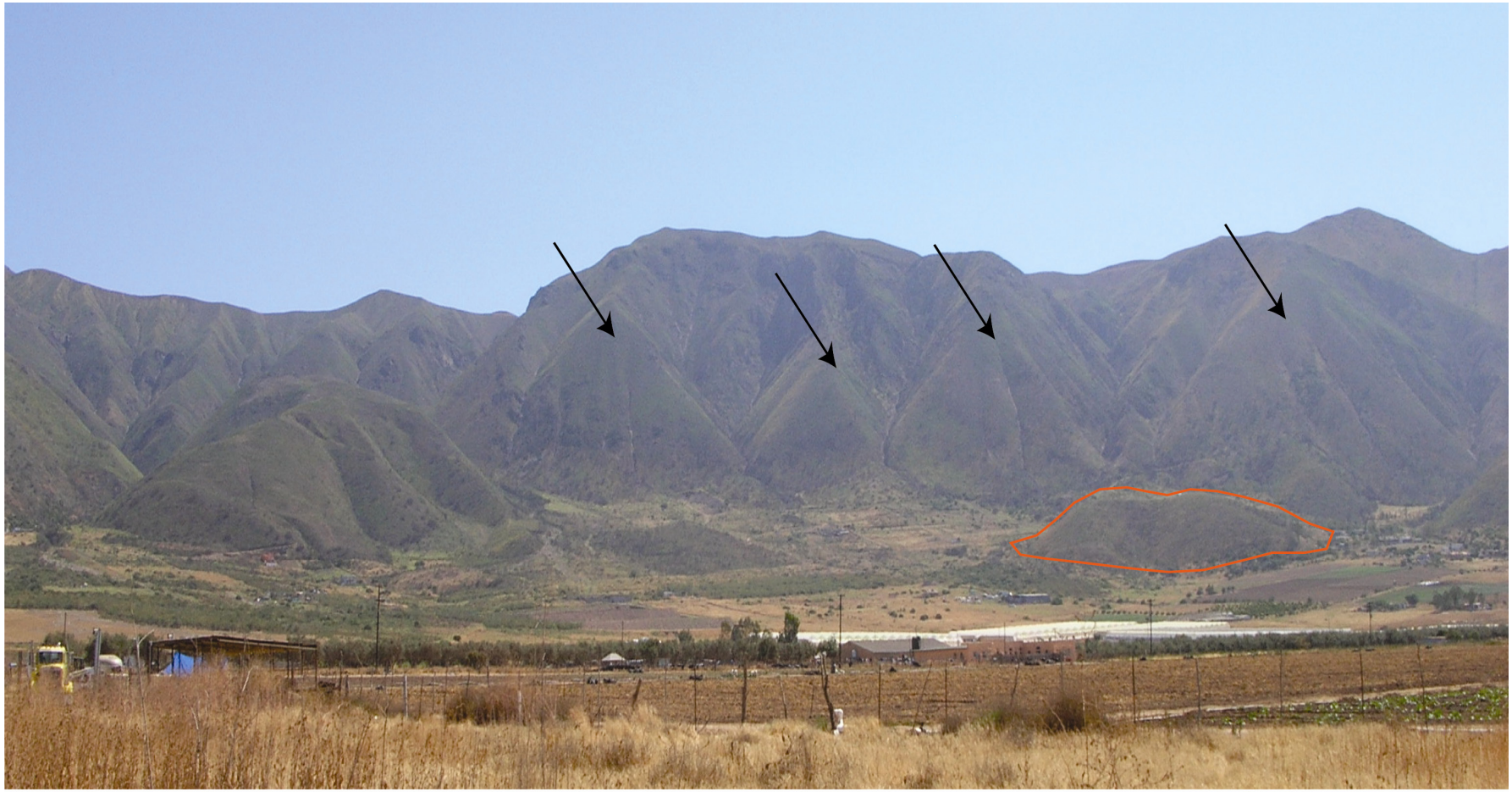

Figure 13. Geomorphic features of Field Area 1: Triangular facets (black arrows) and inferred pressure ridge (orange outline).

Figure 14. Geomorphic feature within FA1: Looking south at deflected stream channel across Fault C. Stream channel is indicated by yellow line.

Figure 15. Geomorphic feature within FA1: Looking east at an exposure of Fault B near the eastern edge of the field area. The approximate fault trace is indicated with the dashed red line. Trees are approximately 2 m tall.

Figure 16. Geomorphic feature within FA1: Looking south at possible fault scarp, approximately 15 m high, along Fault C.

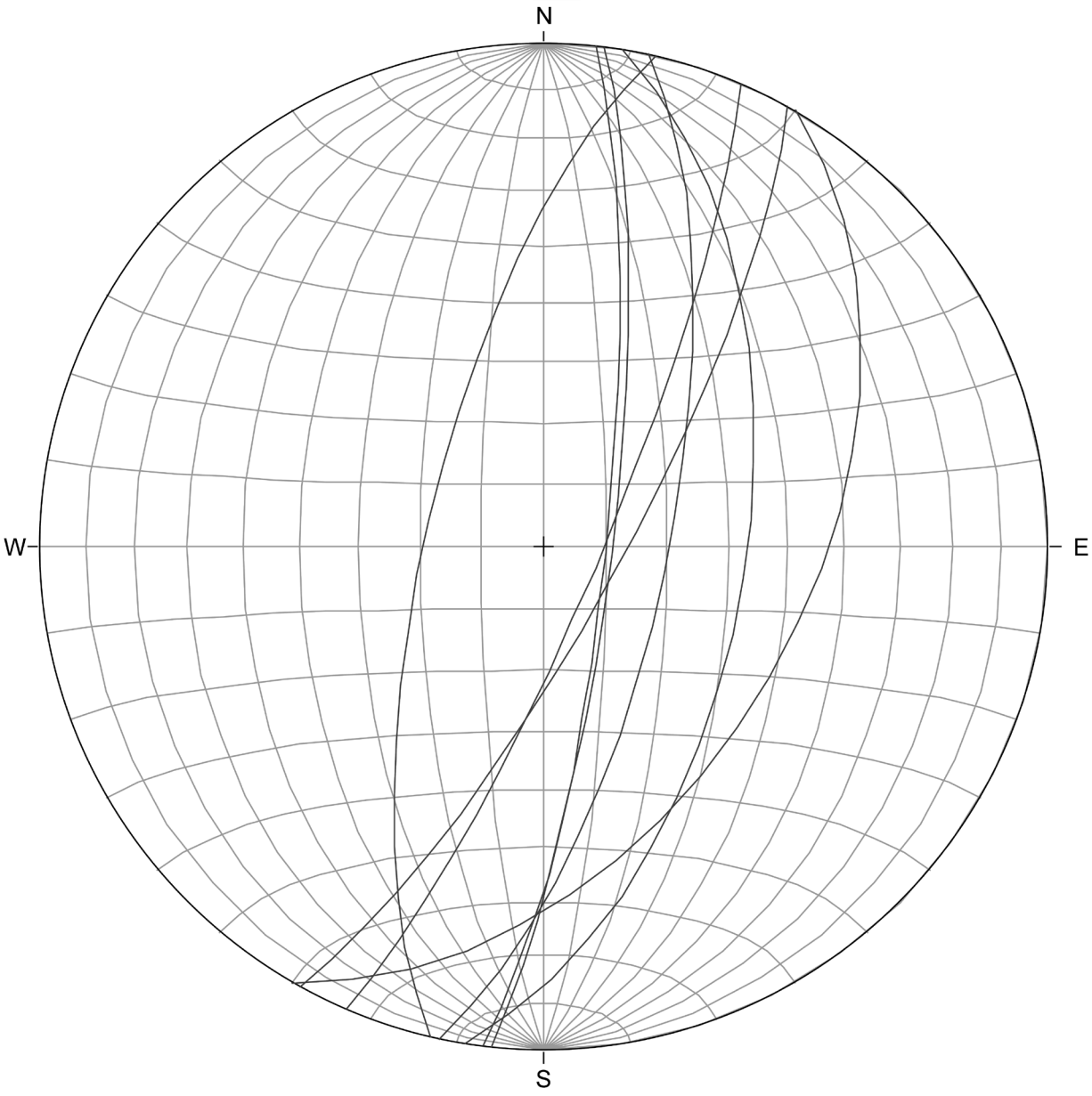

Figure 17. Stereonet of structural data from FA1: north-northeast-south-southwest-trending fractures (n=8).

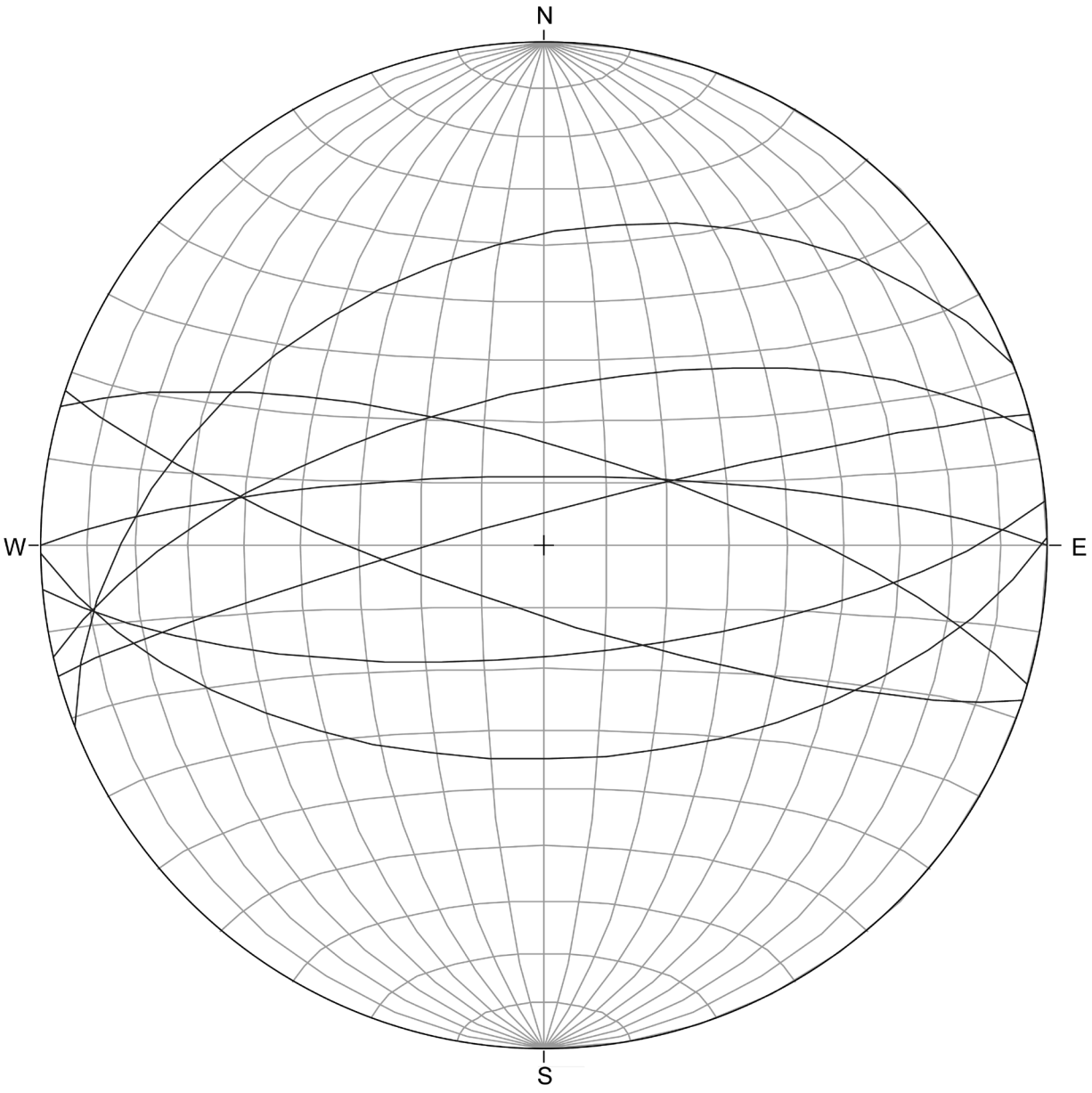

Figure 18. Stereonet of structural data from FA1: east-northeast-west-southwest-trending fractures (n=8).

3.2.1.2 Field Area 2

The second field area (FA2) is located 2 km to the east of FA1 and is mostly within Rancho El Mirador, a ranch with the main ranch house indicated by the green star on the geologic map (Figure 19). Bedrock in FA2 is mostly Alisitos arc volcanic material, although two other units were also identified. About 225 m north of El Mirador, a man-made trail exposes weakly competent, cross-bedded sandstones and conglomerates of the El Rosario Formation with near-vertical dips (Figure 20). Pebbles are mostly well-rounded and composed of volcanic and plutonic clasts. Trough-shaped beds indicate erosional scour. In addition, a previously unmapped tonalite intrusion is located within the volcanic bedrock to the south of El Mirador on Punta Banda ridge and locally forms prominent outcrops (Figure 21). The steep topography limited tracing the entire contact of the intrusion, and the geometry of the pluton was mostly inferred from color changes on the slope. Although the intrusion has not been previously described, the composition is typical for Cretaceous arc-related intrusions in the Peninsular Ranges batholith (e.g., Gastil *et al.*, 1975).

As shown on the geologic map (Figure 19), fault rocks, such as fault breccia and gouge affecting the volcanic bedrock, are located along the main fault trace (Fault A) and a subsidiary fault strand (Fault B) in this field area. Fault A is exposed in a stream channel to the northwest of El Mirador as a 15-m-wide fault breccia zone (Figure 22). The small, angular, volcanic fragments and the matrix within the breccia are light in color. Fault rocks associated with Fault B are found ~390 m farther to the southwest (Figure 23) in the same drainage as the 15-m-wide fault zone along Fault A.

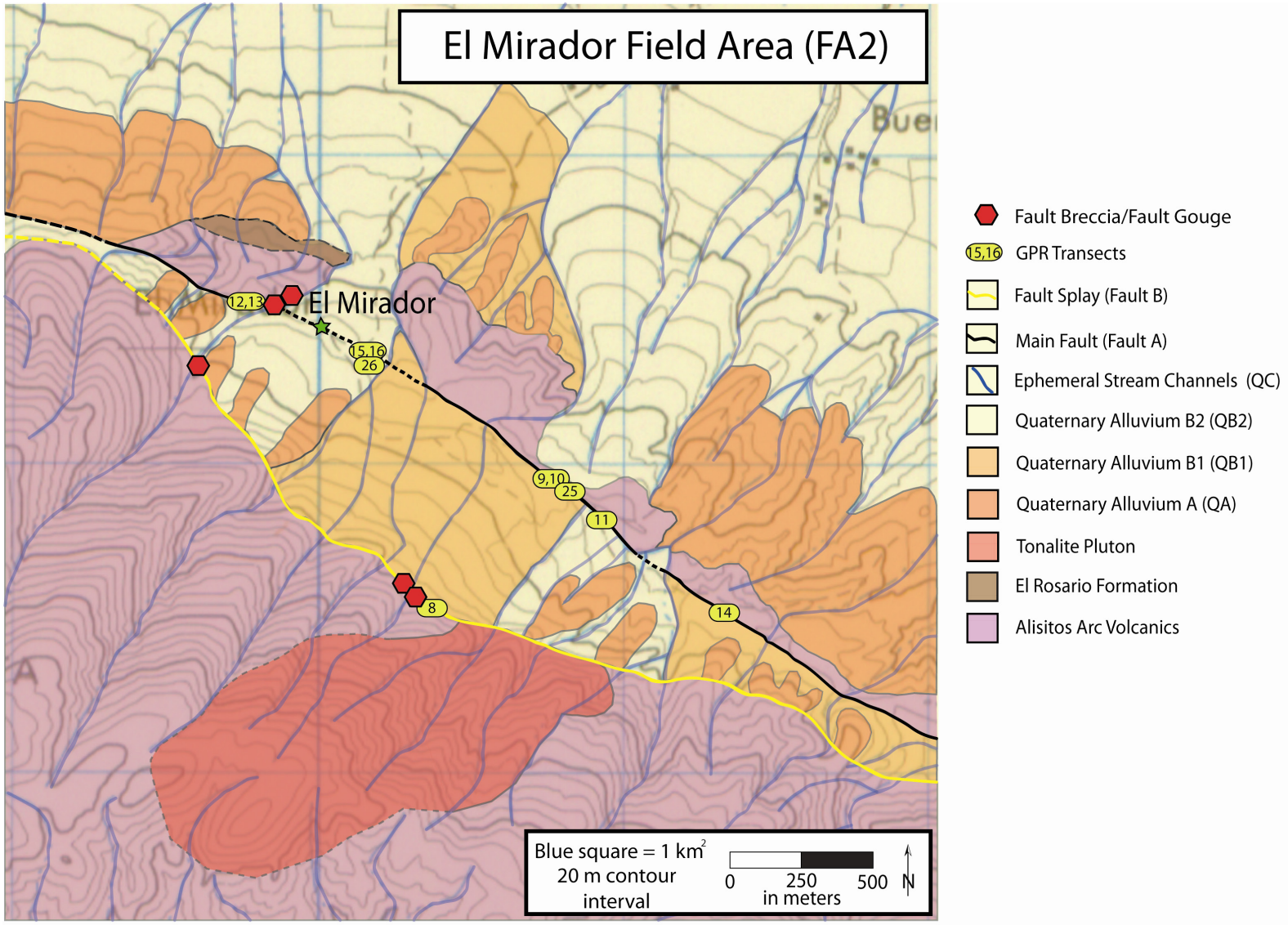

Figure 19. Field map of Field Area 2. Reference point is Rancho El Mirador indicated by the green star. Fault rocks and locations of GPR surveys are indicated as well.

Figure 20. Field photograph of El Rosario Formation outcrop in northwestern FA2. Note the variation in thickness of the pebble beds within the sandy unit. Yellow notebook is 19 cm long.

Figure 21. Tonalite pluton along Fault B within FA2. Tonalite is cut by aplite dike with secondary epidote.

Figure 22. Fault rocks within FA2: Outcrop of breccia 15 m wide indicating location of Fault A at western extent of FA2. The breccia contains volcanic rock clasts ranging from a few millimeters to a few centimeters in length and set in white matrix. Coarse alluvial deposits sit on top. View is to west.

Figure 23. Fault rocks along Fault B within FA2 southeast of El Mirador. Volcanic clasts are multi-colored, generally red, orange and black, and range from a few millimeters to a few centimeters in length. The matrix is orange. Tube for scale is 5 cm long.

FA2 contains a shutter ridge that is only breached in two locations by stream channels that show dextrally deflected courses (Figure 24). This shutter ridge formed as a result of translation of a portion of the volcanic escarpment along Fault A, which bounds the southern edge of this feature. Evidence for a fault splay (Fault B) in the area is shown by the well-developed triangular facets along the mountain front to the south of El Mirador (Figure 25 and 26) as well as dextrally deflected stream channels (Figure 26). Although this secondary splay could not be continuously mapped into FA1, the general trend and location suggest that it may be the eastward continuation of one of the splays from FA1.

As for FA1, stereonets were constructed using fracture measurements from volcanic bedrock located up to several meters south of Fault B within FA2. When plotting the data, two fracture sets emerge. The first set of fractures trends northeast-southwest and shows moderate dips (Figure 27), whereas the second fracture set is at almost right angles, trending northwest-southeast, but with similar moderate dips (Figure 28). In addition, several nonsystematic fractures were measured that apparently do not follow any preferred trend.

3.2.1.3 Field Area 3

FA3 is 2 km east of FA2 along Punta Banda Ridge and is situated adjacent to a steep-walled stream channel (Figure 29) that separates Valle Maneadero and Valle Las Animas, a small valley that ultimately connects with Valle Santo Tomas. An attempt to map this field area in detail was largely unsuccessful, because of poor exposure of bedrock and rugged and treacherous terrain. The main Quaternary units, however, were

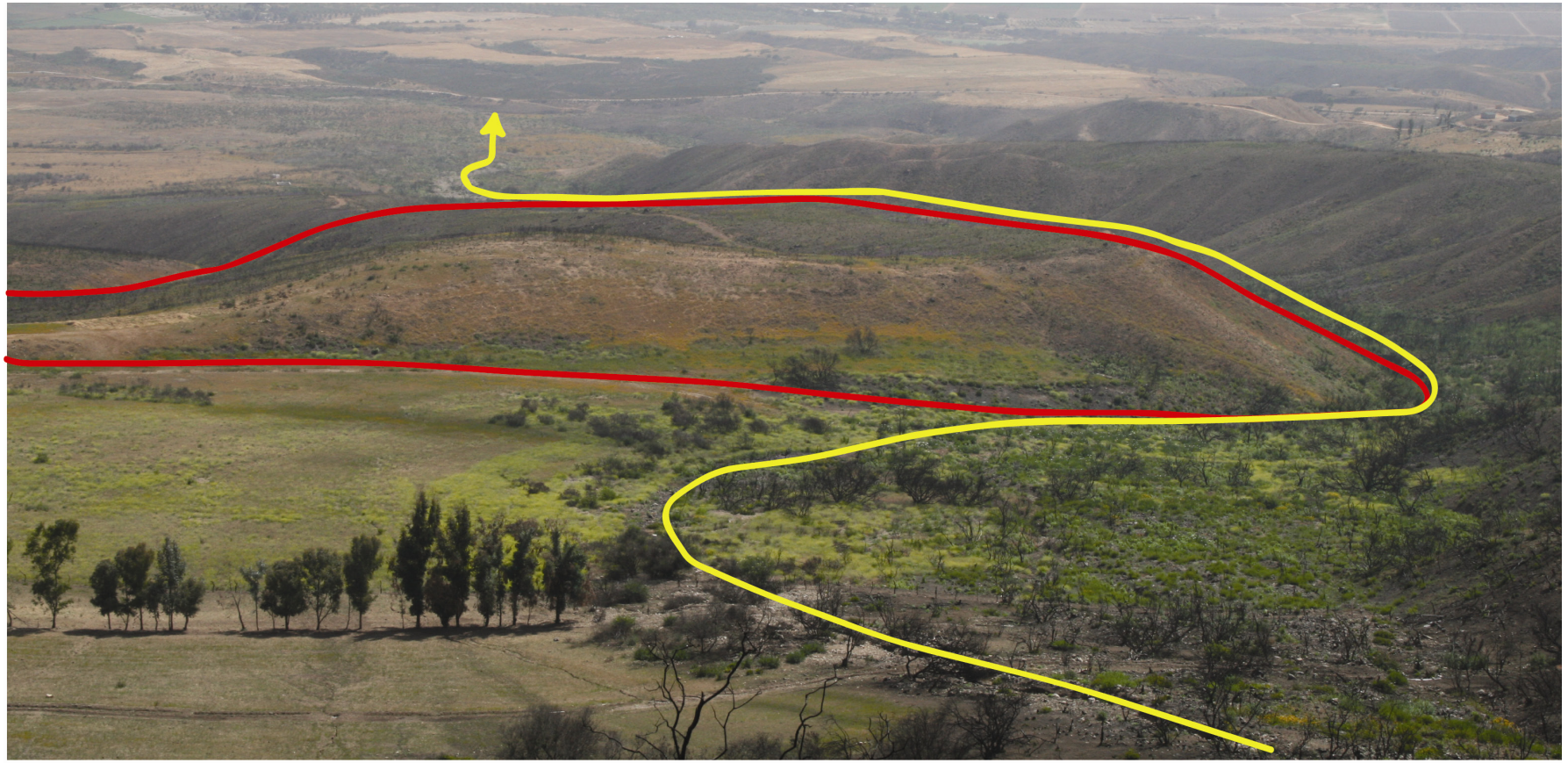

Figure 24. Geomorphic features within FA2: Shutter ridge (outlined in red) caused by translation along Fault A deflects stream channel flowing northward (yellow line).

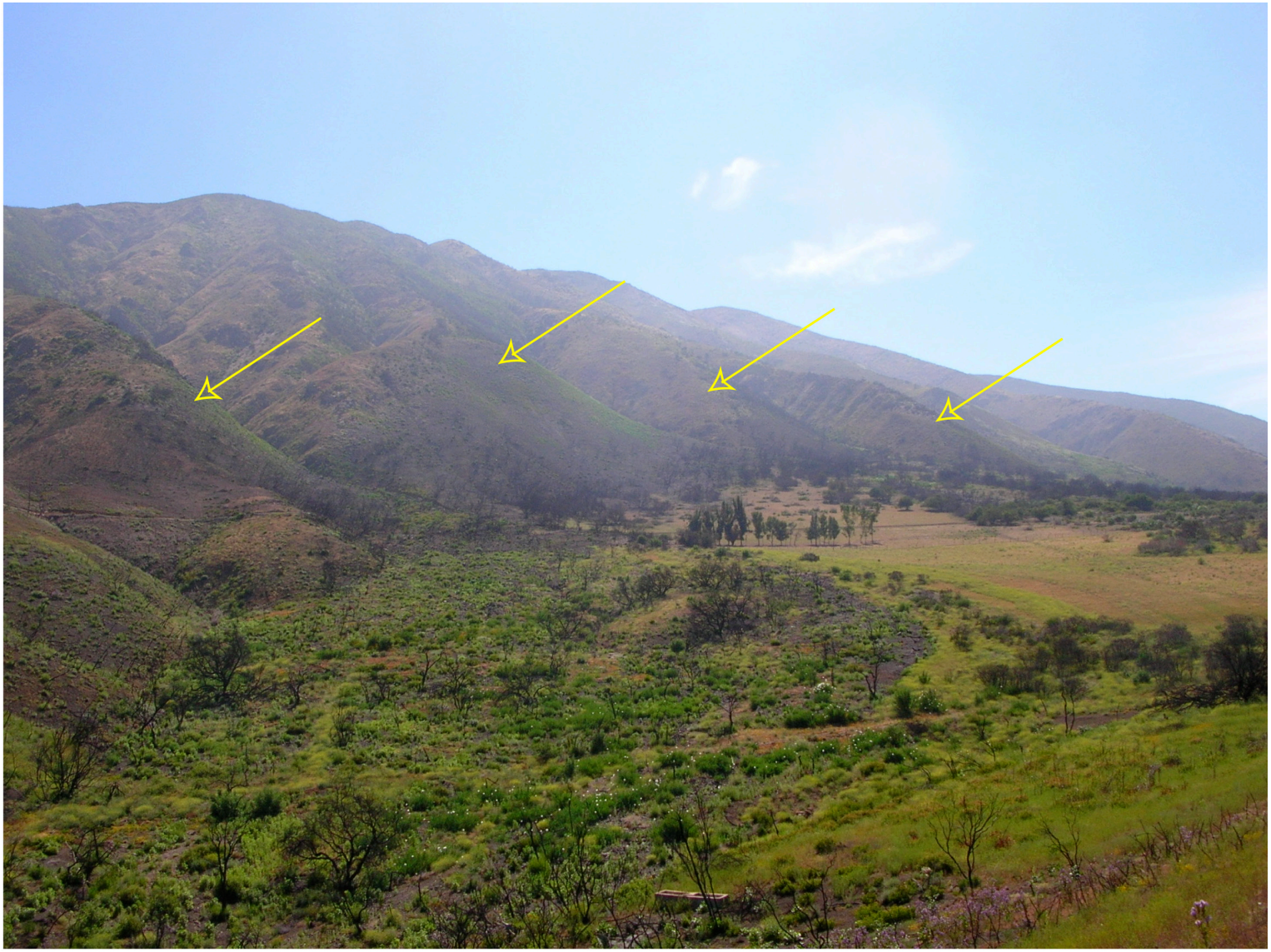

Figure 25. Geomorphic feature within FA2: Poorly developed triangular facets, indicated by yellow arrows, along Fault B. View is to southwest.

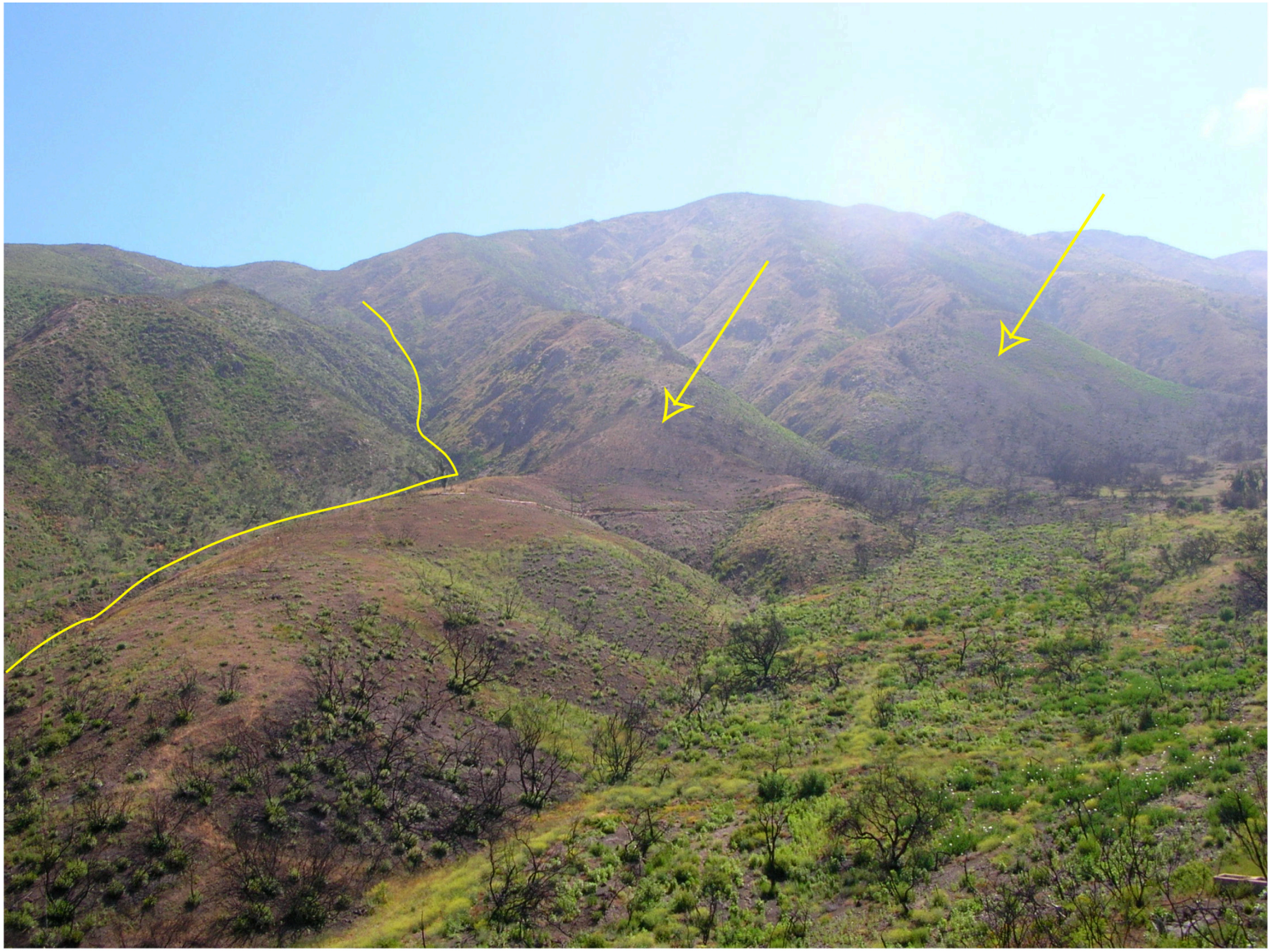

Figure 26. Geomorphic feature within FA2: Deflected stream channel (yellow line) and poorly developed triangular facets, indicated by yellow arrows, along Fault B. View is to southwest.

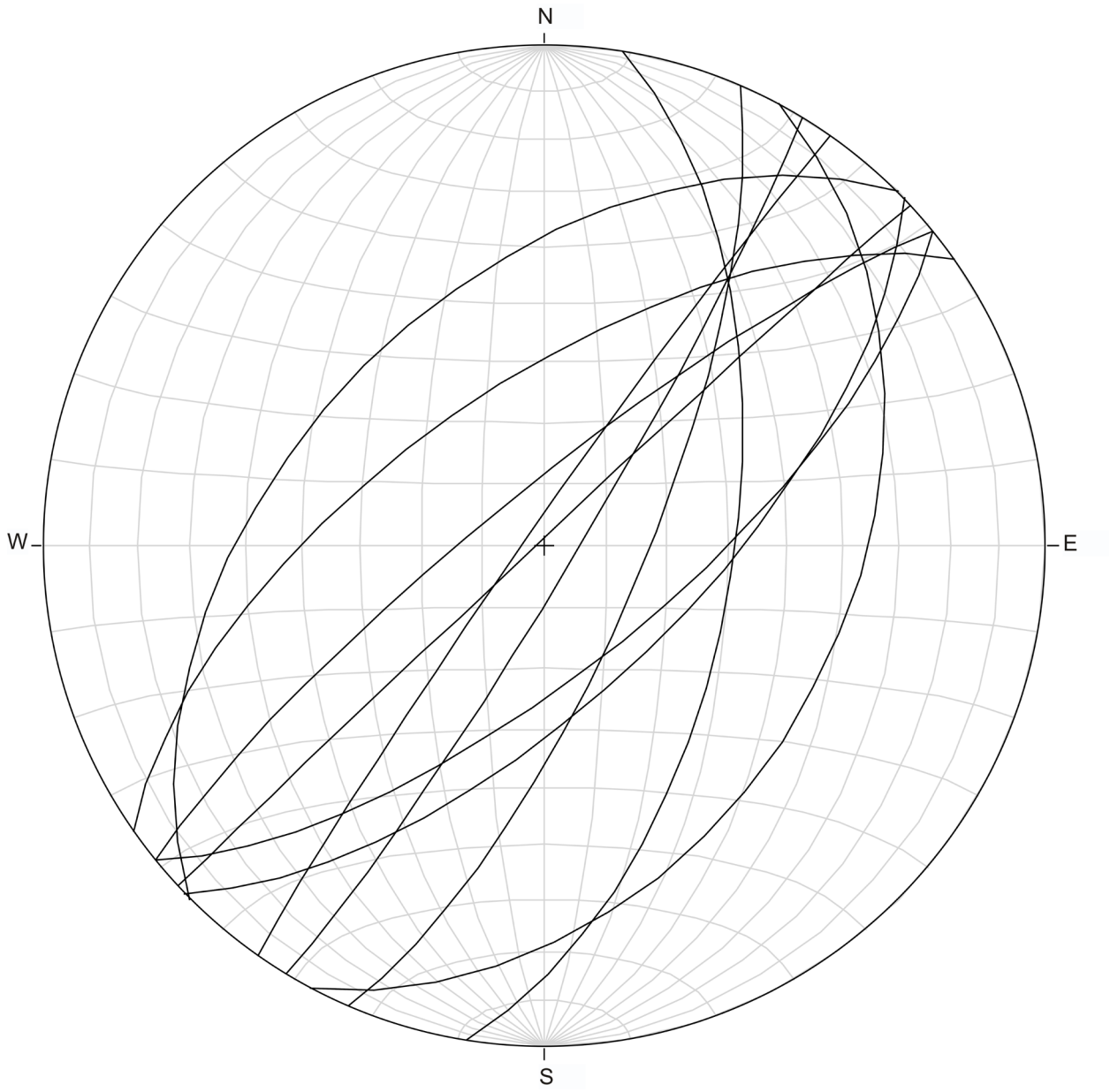

Figure 27. Stereonet of structural data from FA2: northeast-southwest-trending fracture set (n=11).

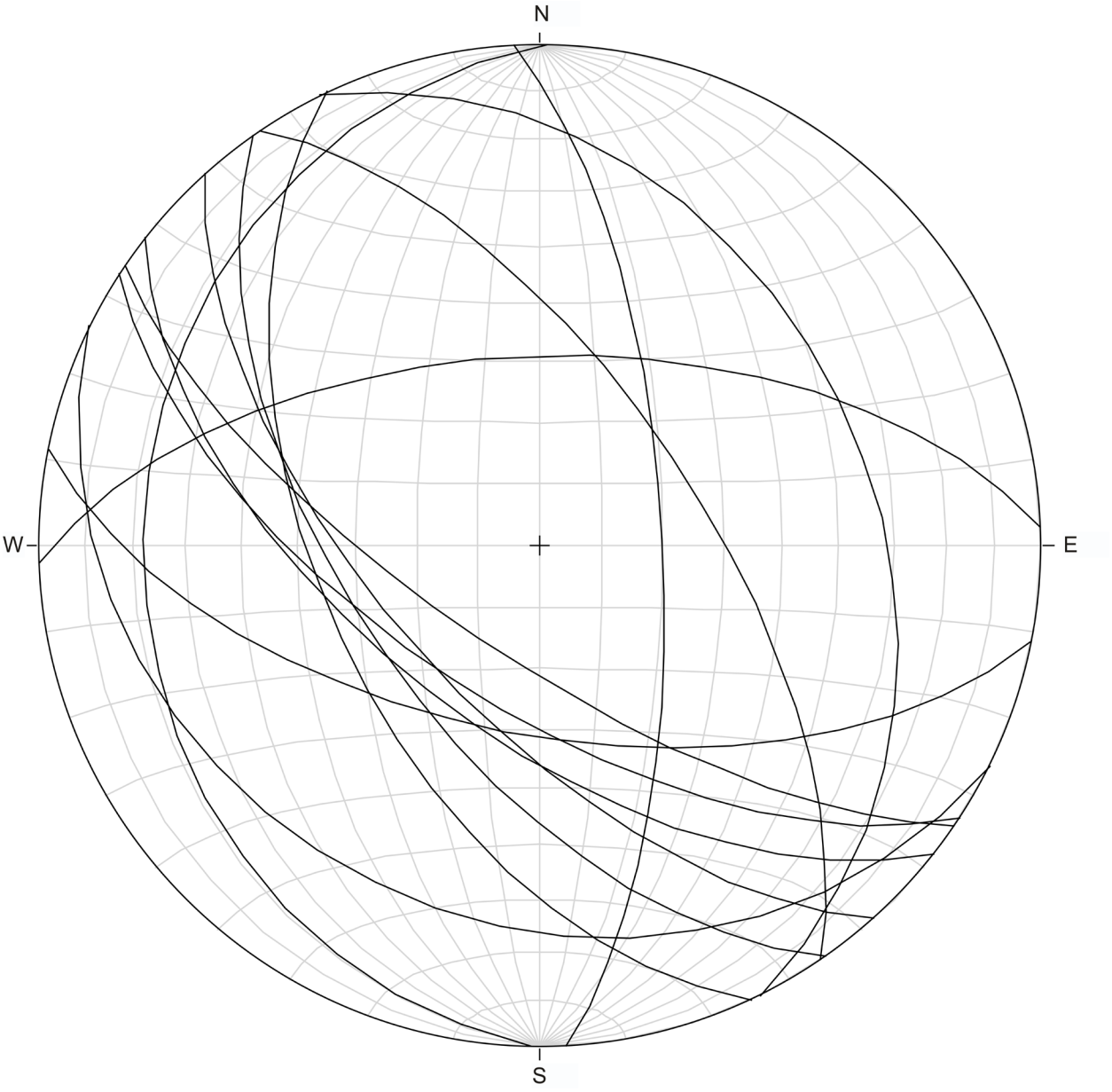

Figure 28. Stereonet of structural data from FA2: northwest-southeast-trending fracture set and nonsystematic fractures (n=13).

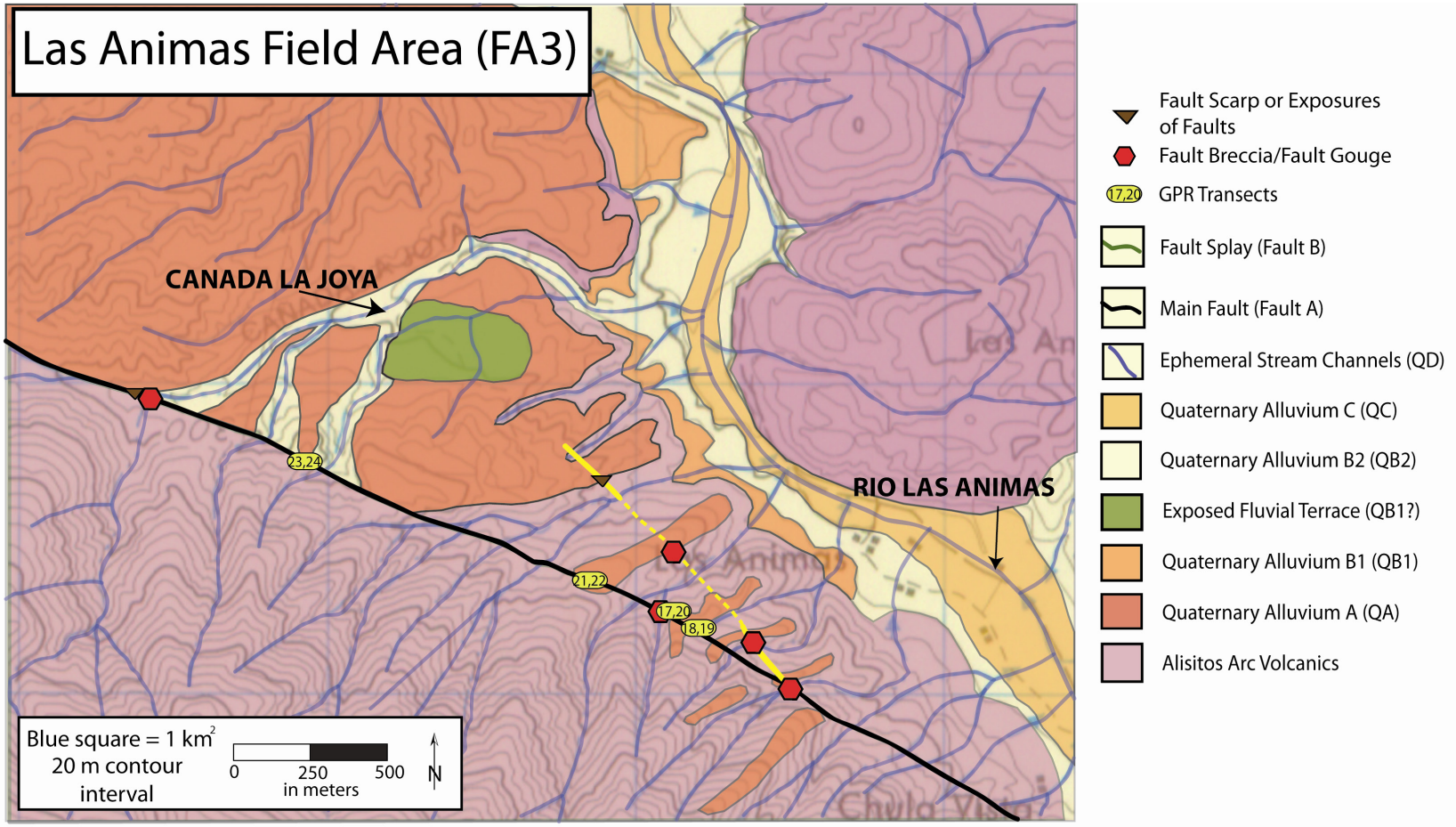

Figure 29. Field map of Field Area 3. Reference points are Canada La Joya in the west and Rio Las Animas in the east. Fault rocks and location of GPR surveys are indicated.

mapped visually from elevated positions in the field area, and geomorphic features (see below) allowed mapping of the main fault trace (Fault A) and a minor fault splay (Fault B).

A drainage exposing fault rocks shows the location of the main fault trace where Canada La Joya intersects the main Agua Blanca fault (Fault A; Figure 30). The fault outcrop, which was inaccessible and was evaluated from a considerable distance, displayed rocks with multi-colored streaks. Although the rocks could not be directly mapped, the trend of the fault rocks with respect to the main fault trace suggests that they represent an exposure of the main fault. Extensive breccia and gouge outcrops were also found within drainages adjacent to groves of trees at the northeastern edge of the field area. The breccia is characterized by angular, light-colored volcanic fragments within a red and orange matrix (Figure 31). The fault gouge is composed of bright red, orange and black particles (Figure 32). In the eastern part of the field area, Fault B extends northwestward from the main fault (Figure 29). Fault B was traced through three outcrops of fault rocks which fall along a straight line. The trace of Fault B is lost to the northwest in the surrounding hills, which are composed of alluvium.

In FA3, Fault A shows poorly developed triangular facets along the mountain front (Figure 33). Ridges of volcanic bedrock covered with a veneer of alluvium extend from the mountain front and are cut by deep stream channels. Deflection within these stream channels also signifies the trace of Fault A. The fault also provides a pathway for groundwater flow. Springs have formed along the fault as a result, and a prominent line of trees occur along the main fault trace (Figure 34). A prominent fluvial terrace to the

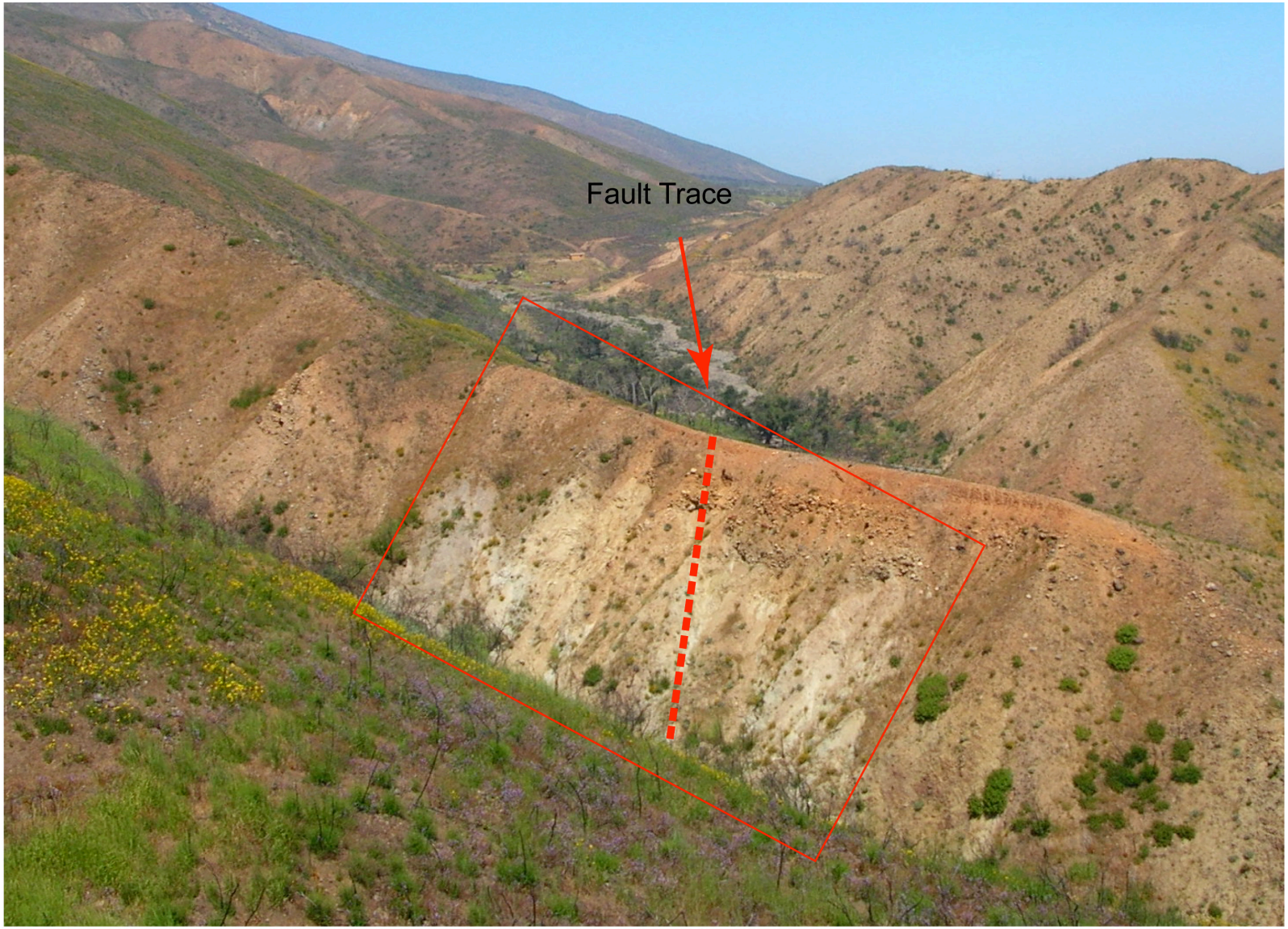

Figure 30. Modern drainage at the western edge of FA3 exposes fault breccia and gouge indicated by multi-colored white, red and orange bands within the red box at the center of the photograph. View is looking west along the Agua Blanca fault toward FA2. Dashed red line indicates possible location of the main fault trace.

Figure 31. Fault rocks within FA3: Fault breccia along Fault A southeast of Canada La Joya. White, angular volcanic clasts are a few millimeters to a few centimeters in size and are set in an orange and red matrix. Hammer for scale.

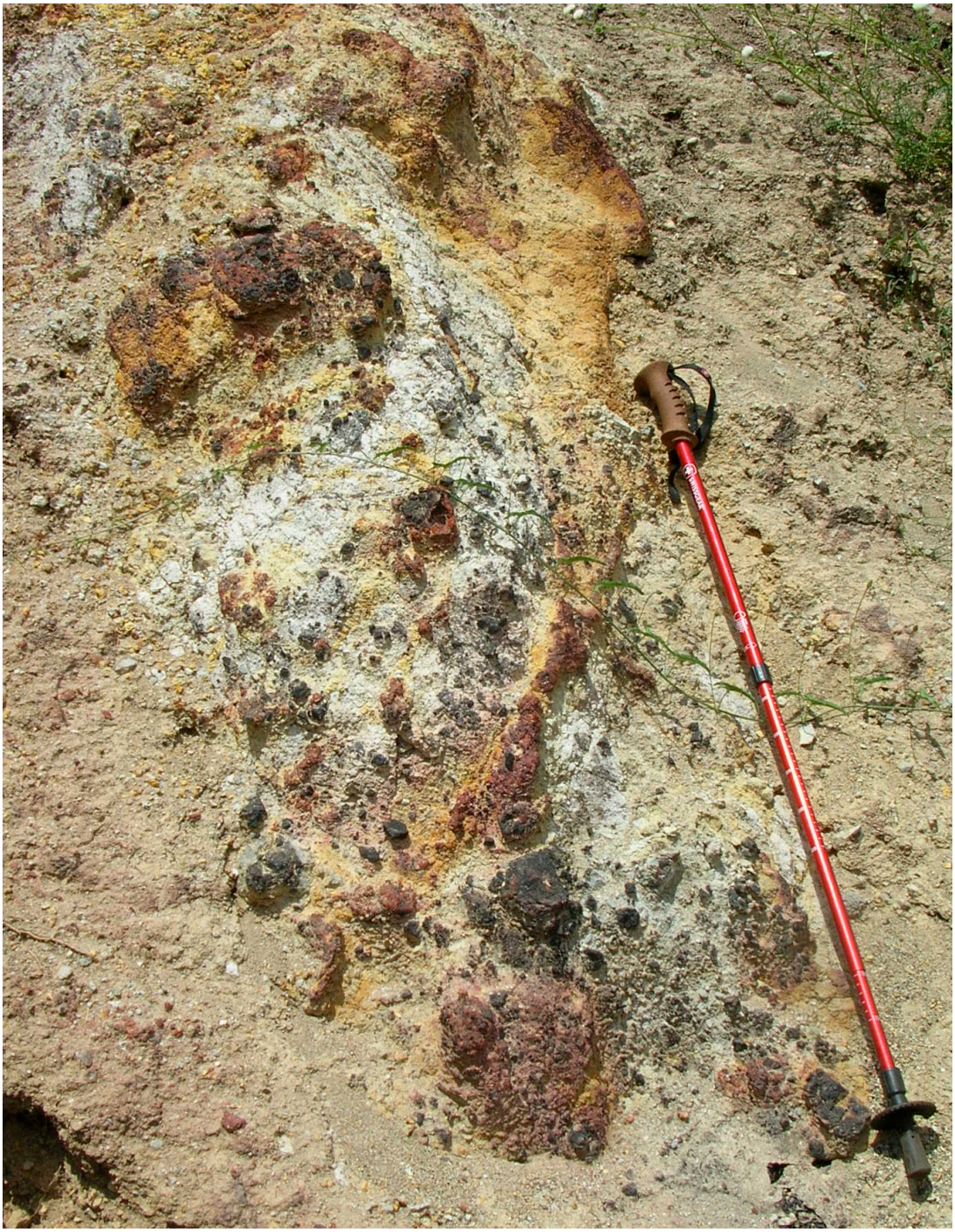

Figure 32. Fault rocks along Fault A southeast of Canada La Joya. Volcanic clasts are orange, red and black in color and a few millimeters to several centimeters in size. The matrix is white to orange. Walking stick for scale.

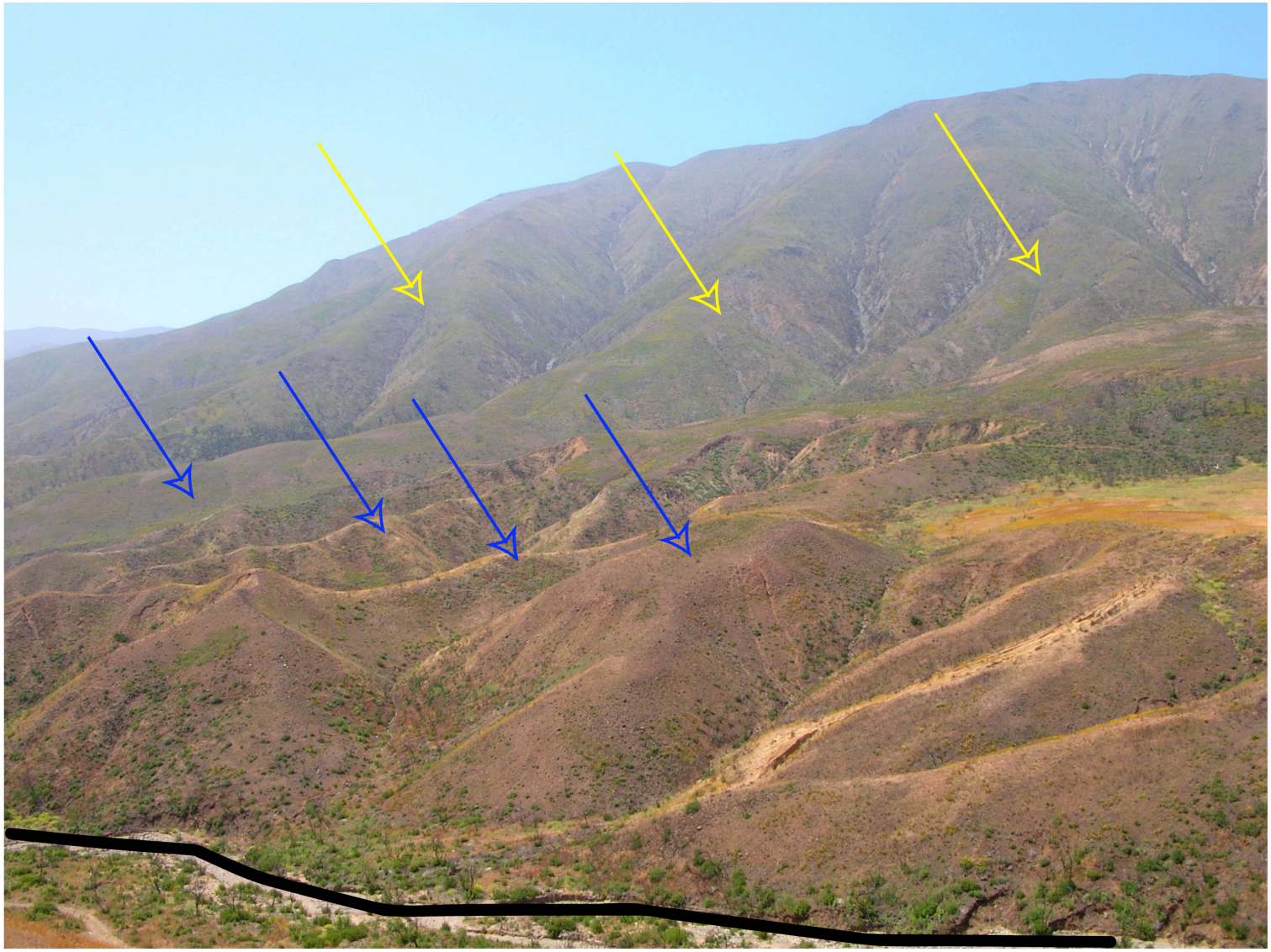

Figure 33. Geomorphic features within FA3: Poorly developed triangular facets, indicated by yellow arrows, along Fault A. Ridges of volcanic rock, indicated by blue arrows, are covered with alluvium and cut by deep stream channels such as Canada La Joya, indicated by the black line. View is to east-southeast.

Figure 34. Alignment of trees along Fault A in FA3. Fault trace is indicated by black dashed line. View is to south.

east of Canada La Joya indicates a former base level (Figures 29 and 35), and several small fluvial terraces are directly adjacent to the Rio Las Animas, which is the main currently active channel (Figure 36).

3.3 Classification of Quaternary Alluvium

Quaternary units in the study area are divided into four groups (QA, QB, QC, QD) based on successive depositional relationships observed in drainages and variation in topographic expression. The naming convention is based on similarity of topography and does not imply coeval deposition in each of the field areas. Most of the currently active stream channels are reworking older alluvial fan deposits by incising and eroding units QA and QB. Many of these channels are less than 2 m deep, indicating that they became active recently.

In FA1, unit QA was initially deposited as alluvial fans along the mountain front. It is likely that the deposits were more extensive in the past and the fans may have coalesced to form a ramp. An increase in the gradient of the slope, which likely resulted from a drop in base level, led to increased erosion upstream of the main fault. Base-level drop resulted in the dissection of unit QA and formation of unit QB. Similarly, a renewed drop in the base level caused incision and erosion of QB and formation of the currently active stream channels (QC).

The age relationships of Quaternary deposits in FA2 are slightly more complex. Unit QA was deposited as alluvial fans along the mountain front. However, the presence of the shutter ridge in the area resulted in limited incision of QA deposits when base level dropped. Thus, sediment (QB1) was trapped behind the shutter ridge until the

Figure 35. Geomorphic features within FA3: Exposed fluvial terrace, indicated by blue arrow, and deep stream channel named Canada La Joya.

Figure 36. Geomorphic features in FA3: Fluvial terraces, indicated by yellow arrows, developed along Rio Las Animas, the main currently active channel. View is to northwest.

ridge was breached. At that point in time, sediment was no longer confined and areas of alluvial deposits were quickly reworked to reach the new lower base level. Units QA and QB1 were dissected and redeposited in the valley, forming QB2. Renewed lowering of the base level caused continued incision of QA and QB1, started incision of QB2, and led to the formation of the youngest unit, QC.

The age relationships between the Quaternary deposits in FA3 are less certain, as less time was spent in the area. QA was likely deposited as alluvial fans. When base level dropped, QA began to be dissected and QB1 was deposited as alluvial fans and fluvial terraces. It is possible that the exposed fluvial terrace that sits atop QA adjacent to Canada La Joya (Figure 35) is part of QB1. With successive base level drops, the QB1 fluvial terraces were incised and the unit was reworked. Similarly the formation and erosion of QB2 and QC are probably related to successive base level drops, before the current stream channel began depositing QD.

3.4 GPR Sections and Interpretations

3.4.1 GPR survey locations and reflector descriptions

The GPR system utilized for this project was a pulseEKKO 100 designed by Sensors and Software Incorporated. The DVL and the control unit (see p. 6) are attached to a backpack for transportation to desired survey locations. Between the two antenna sizes (50 and 100 MHz) available for use with this system, I chose to use the smaller, higher frequency 100 MHz antennae for two reasons: 1) they were easier to wield on steep terrain, and 2) have elsewhere been used successfully as a compromise between depth of penetration and signal resolution (Yetton and Nobes, 1998; Slater and Niemi, 2003).

Thirty GPR surveys were divided among the three field areas. Using a 0.25 m step size, ten reflection surveys (transects 1-7, 27-29) and one CMP survey (transect 30) were completed within FA1 (Figure 10). Seven reflection surveys (transects 8, 10-12, 14-16) and four CMP surveys (transects 9, 13, 25-26) were completed within FA2 (Figure 19). Four reflection surveys (transects 17-18, 22-23) and four CMP surveys (transects 19-21, 24) were completed within FA3 (Figure 29). Time zero calibrations were made before sampling each location, confirming that the first trace recorded coincides with the arrival of the first radar wave. Certain parameters were used for all transects, such as a sampling interval of 801 picoseconds (ps), a time window of 433 nanoseconds (ns) and an auto gain function. Different stacking arrangements of the signals were applied, but only affected the display on the DVL and did not influence the raw data. Each transect was tracked using one or two GPS handheld devices (Garmin eTrex H and Garmin Colorado 400t). Survey start and end points were marked and each transect was continuously tracked.

The GPR data were downloaded from the DVL onto a personal computer. Two programs from Sensors and Software Incorporated, EKKO_View Deluxe and EKKO_View, were used to process the data and view the sections, respectively. Longitude and latitude GPS data were applied to each transect and topography was corrected using elevation data. The GPR data were filtered for “wow”, a false low frequency that is superimposed on the high frequency reflections. “Dewowing” the data removes the low frequencies while preserving the high frequencies. A spreading and exponential compensation (SEC) gain was applied to the data, which attempts to compensate for signal spreading loss due to the sphericity of the Earth and exponential

dissipation of signal energy. A color scale was also applied to the sections to bring out subtle nuances in the data to aid in interpretation.

3.4.2 Interpretation of GPR sections

The first two signals at the top of each GPR section were disregarded as they represent the air and ground wave, respectively, and not the subsurface section. Sections were analyzed for two components: alluvial deposits indicated by continuous, discontinuous, wavy, chaotic and parabolic lateral reflectors, and vertical displacement of these lateral reflectors representing potential fault surfaces. The classification of alluvial reflectors within the GPR sections is modeled after the definitions by Ekes and Friele (2003) (Figure 37). The results of the GPR surveys were mixed. Many of the sections provided less than 5 m depth of penetration, with minor portions of the section for interpretation. However, decent depth penetration was achieved in a few sections from each field area and those sections are described below.

In FA1, only one section, Line 3 (Figure 38) across Fault C (Figure 10), was analytically viable. The alluvial reflectors showed a variety of characteristics. The convex reflector (red arrow) in this section could be indicative of trees. When the transmitter sends the EM signal, a portion of the signal travels along the surface and is captured by the receiver. When the signal strikes an object at the surface, the signal can become contorted and can superimpose an interference figure, such as a convex reflector, on subsurface sections of the survey (Burger *et al.*, 2006). Although there were no trees on the surface at this location due to a fire the previous year, we noted many stumps left behind which could be causing interference.

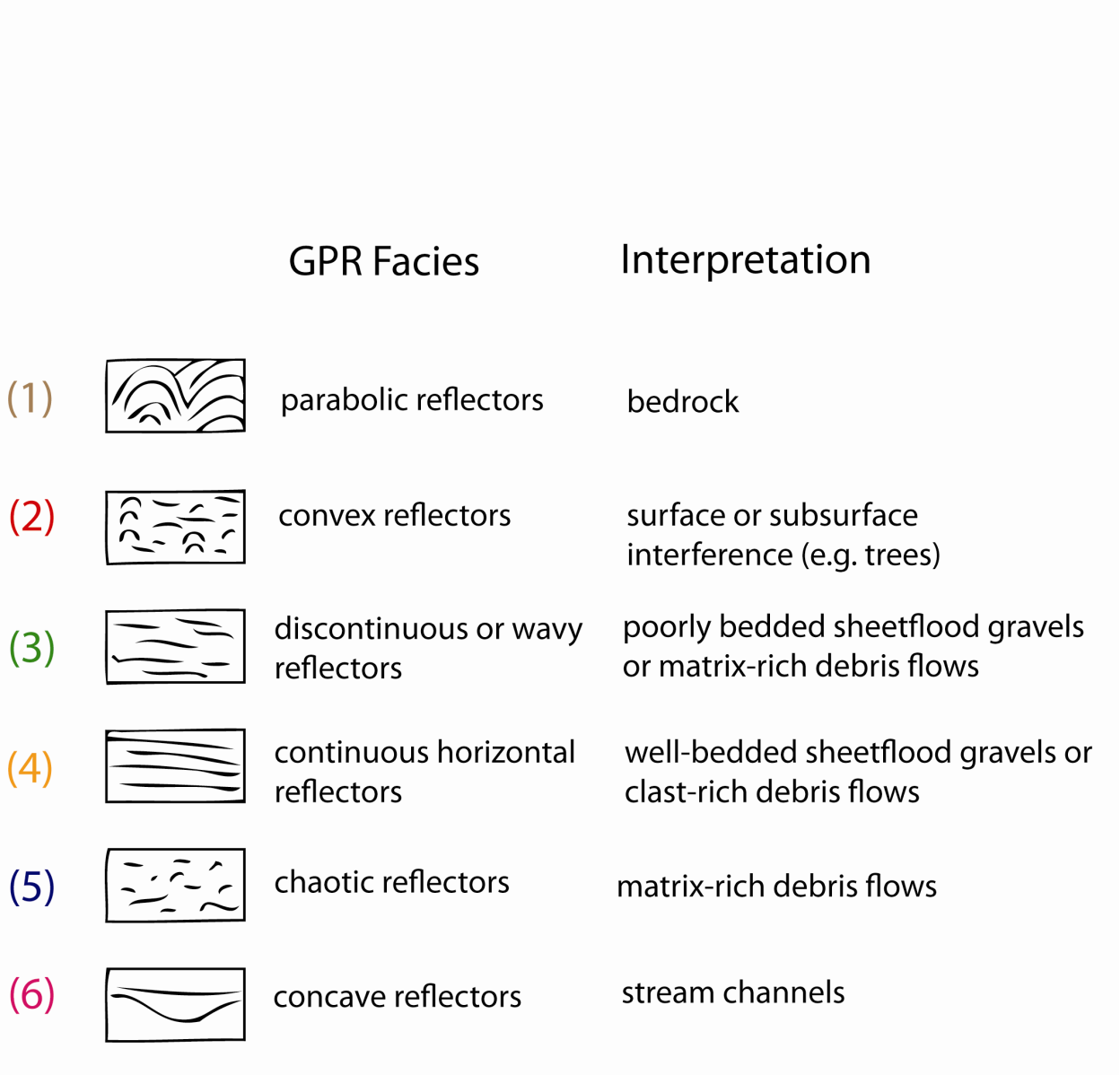

Figure 37. GPR Facies as modeled by Ekes and Friele (2003). Colored numbers correspond with colored arrows incorporated in GPR section figures.

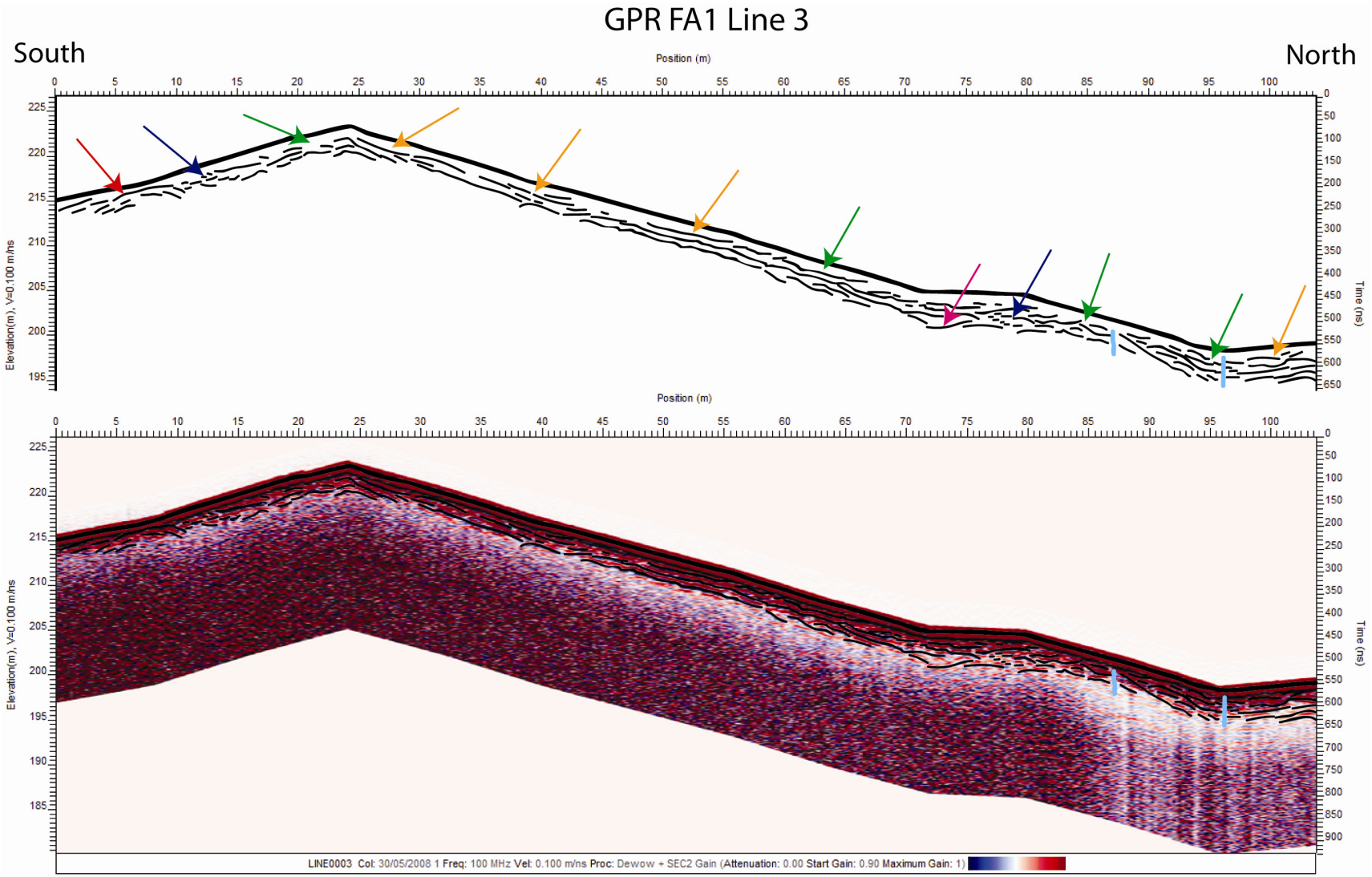

Figure 38. GPR transect within FA1: Line 3. Colored arrows correspond with GPR radar facies by Ekes and Friele (2003), as seen in Figure 37.

The blue arrows signify a chaotic debris-flow deposit, probably emplaced during a flood. The green and orange arrows indicate increasing order and structure within sheet-type gravel units. The pink arrow indicates a concave reflector that could signify a small stream channel. Two fault traces (blue vertical lines) were identified near the northern end of the section based on pervasive vertical disruption of lateral reflectors. The northernmost fault within this section corresponds with the trace of Fault C.

Three surveys from FA2 were analyzed (Figure 19). Line 8 (Figure 39) crosses Fault B and Lines 15 and 16 (Figure 40 and 41) cross Fault A. In Line 8 (Figure 39), the alluvial reflectors near the south end of the section are slightly convex (red arrow), chaotic (blue arrows) or slightly concave (pink arrow). These patterns are inferred to represent tree interference, debris-flow deposits and possibly a small stream channel, respectively. The reflections become more ordered northward; the green and orange arrows indicate poorly bedded and well-bedded sheetflood gravels, respectively. Many more potential fault traces are visible within this section than are visible at the surface, which suggests that undisturbed alluvial deposits might cover subsidiary fault splays. A cluster of faults is located ~40 m northward from the beginning of the transect with another smaller cluster at the 60 m mark. Two single fault traces are evident at 72 and 82 m, and it is likely that one of these faults represents the main fault trace (Fault A). I interpret the trace at 72 m to be the main fault trace (Fault A), because surface mapping suggests that a change in topography is commonly associated with the fault trace. Alluvial deposits on line 15 (Figure 40) show less organization; only chaotic debris-flow deposits (blue arrows) and poorly bedded sheetflood gravels (green arrows) are apparent in this section. This unorganized signature could be related to obstruction

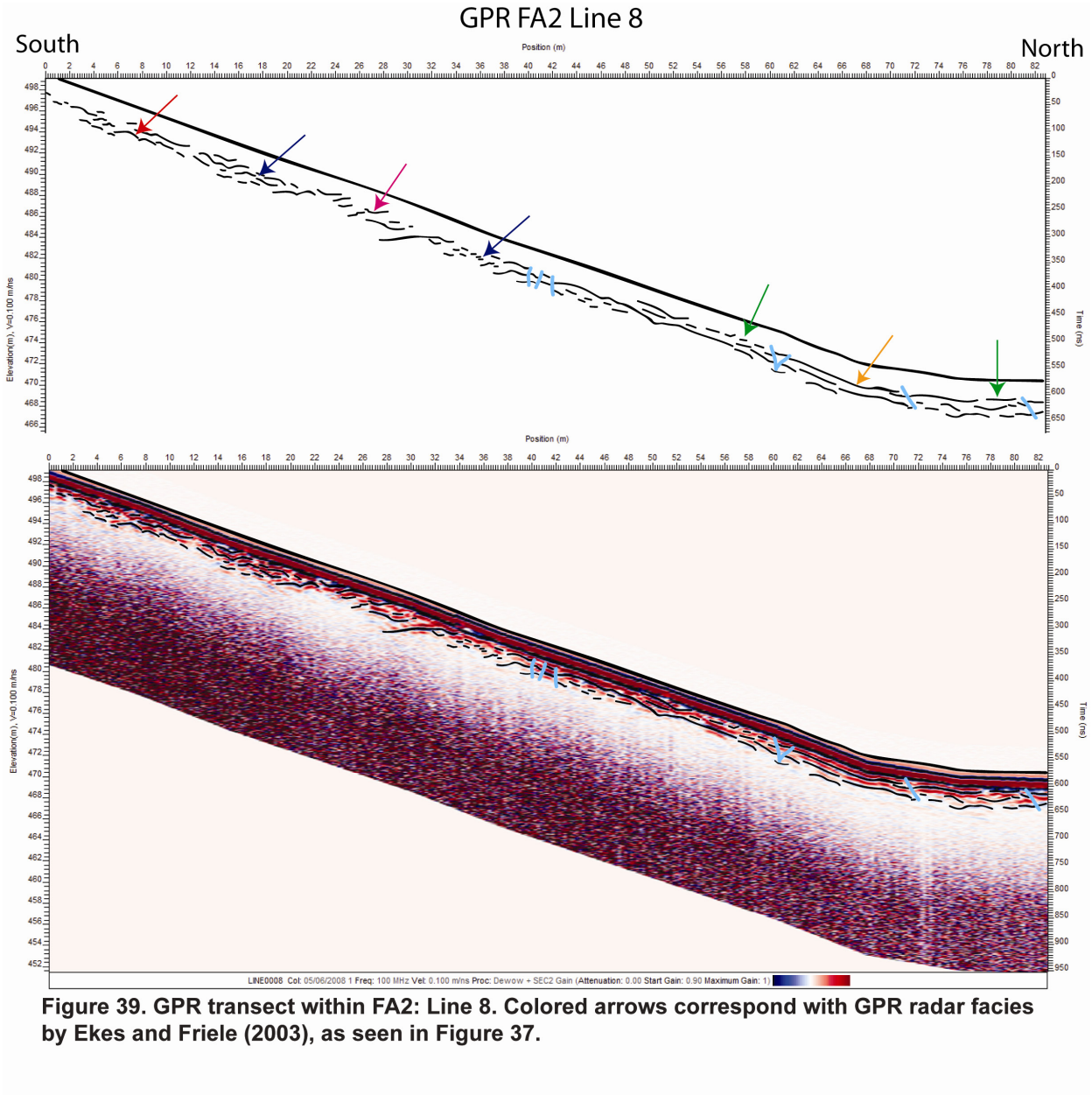

Figure 39. GPR transect within FA2: Line 8. Colored arrows correspond with GPR radar facies by Ekes and Friele (2003), as seen in Figure 37.

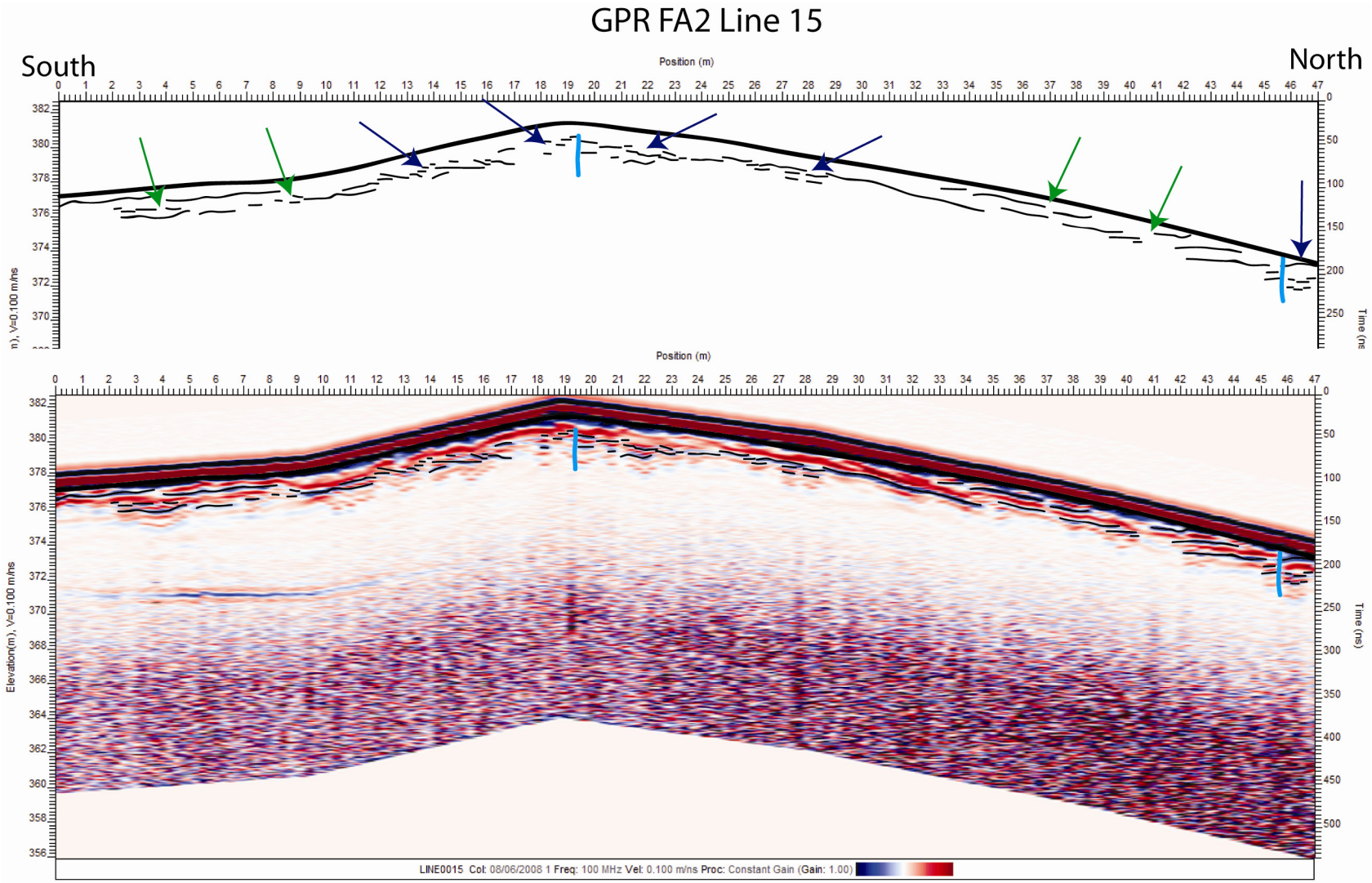

Figure 40. GPR transect within FA2: Line 15. Colored arrows correspond with GPR radar facies by Ekes and Friele (2003), as seen in Figure 37.

of sediment flow by the shutter ridge. Only two potential fault traces, at 19 and 46 m, are visible, and the more northward of the two would correspond to the main fault trace (Fault A). Line 16 (Figure 41) is the northern continuation of Line 15 and is dominated by poorly bedded to parallel-bedded sheetflood gravels.

Two sections, Lines 17 and 22, were analyzed from FA3 (Figure 29). Line 17 (Figure 42) shows changes between signatures for sheetflood gravel (green and orange arrows) and chaotic debris-flow deposits (blue arrows). Two probable fault traces are present. The northern fault represents the main fault trace based on the abrupt topography change, and the southern trace is inferred to be a secondary fault splay. The quality of the traces within Line 22 (Figure 43) is worse than in most of the sections. The poor quality and high concentration of parabolic interference forms (brown arrows) in the southern portion of the section can be attributed to bedrock; the continuity, concentration, and size of signatures point to a larger source than trees (c.f., Ekes and Friele, 2003). If all the discontinuities in the section are in fact fault traces, then the fault system is quite complex and several optional locations for the main fault trace are possible. The three areas of abrupt topographical change, around 50, 80 and 115 m, show corresponding faults. I interpret the southernmost cluster of faults, around 50 m, as the main fault trace due to the steep topography to the north, which limited the area where the transect could be captured.

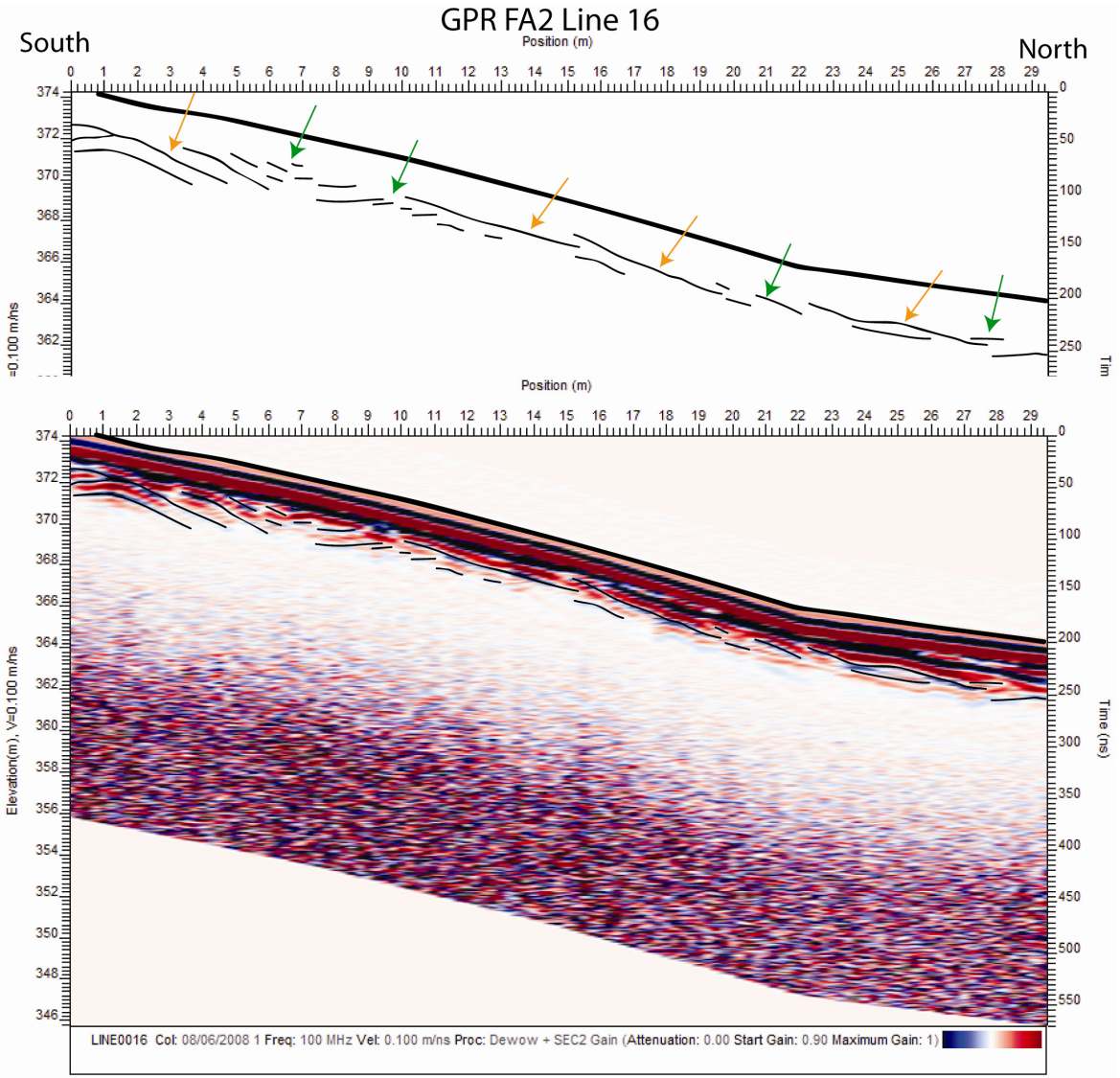

Figure 41. GPR transect within FA2: Line 16. Colored arrows correspond with GPR radar facies by Ekes and Friele (2003), as seen in Figure 37.

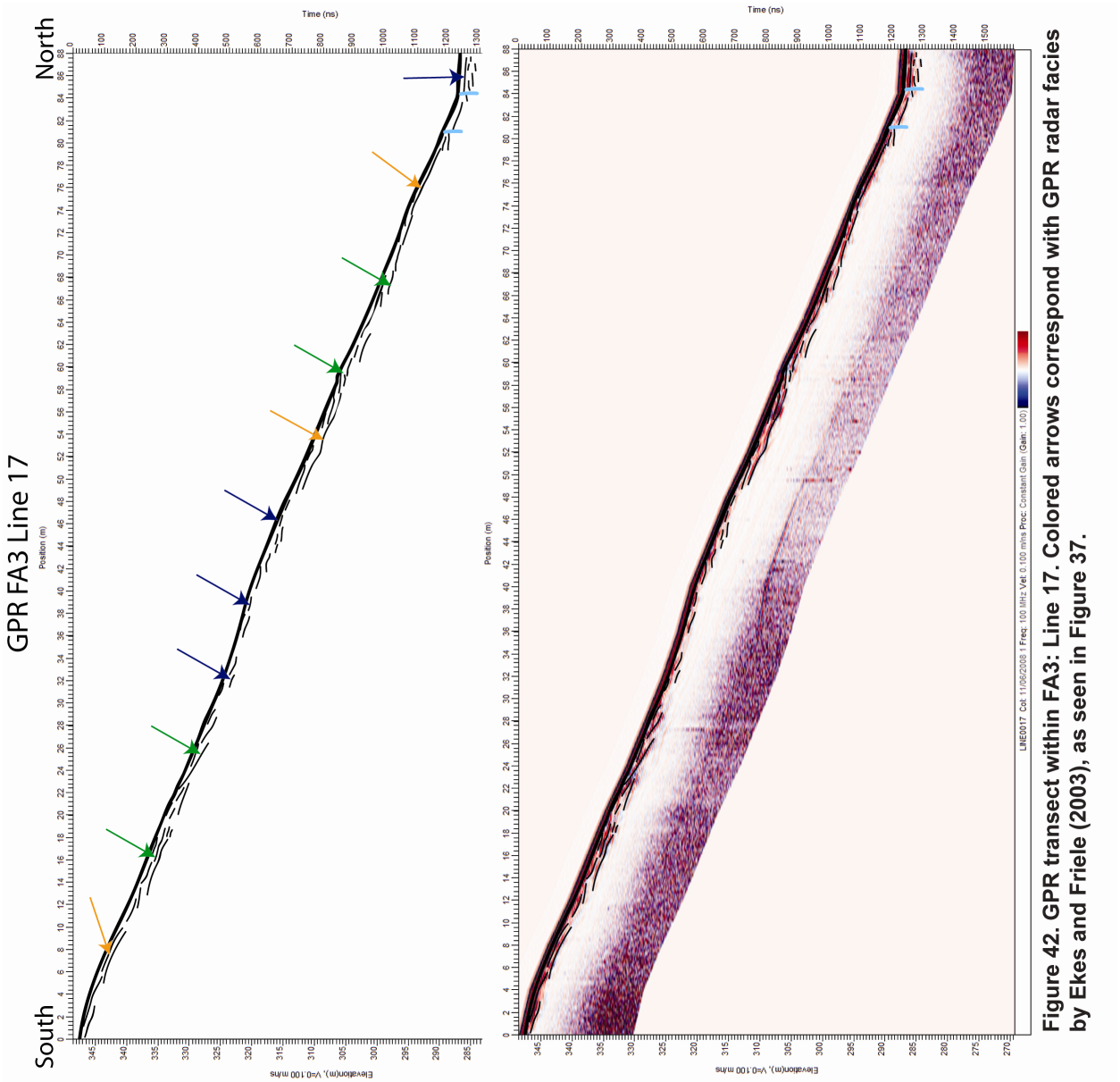

Figure 42. GPR transect within FA3: Line 17. Colored arrows correspond with GPR radar facies by Ekes and Friele (2003), as seen in Figure 37.

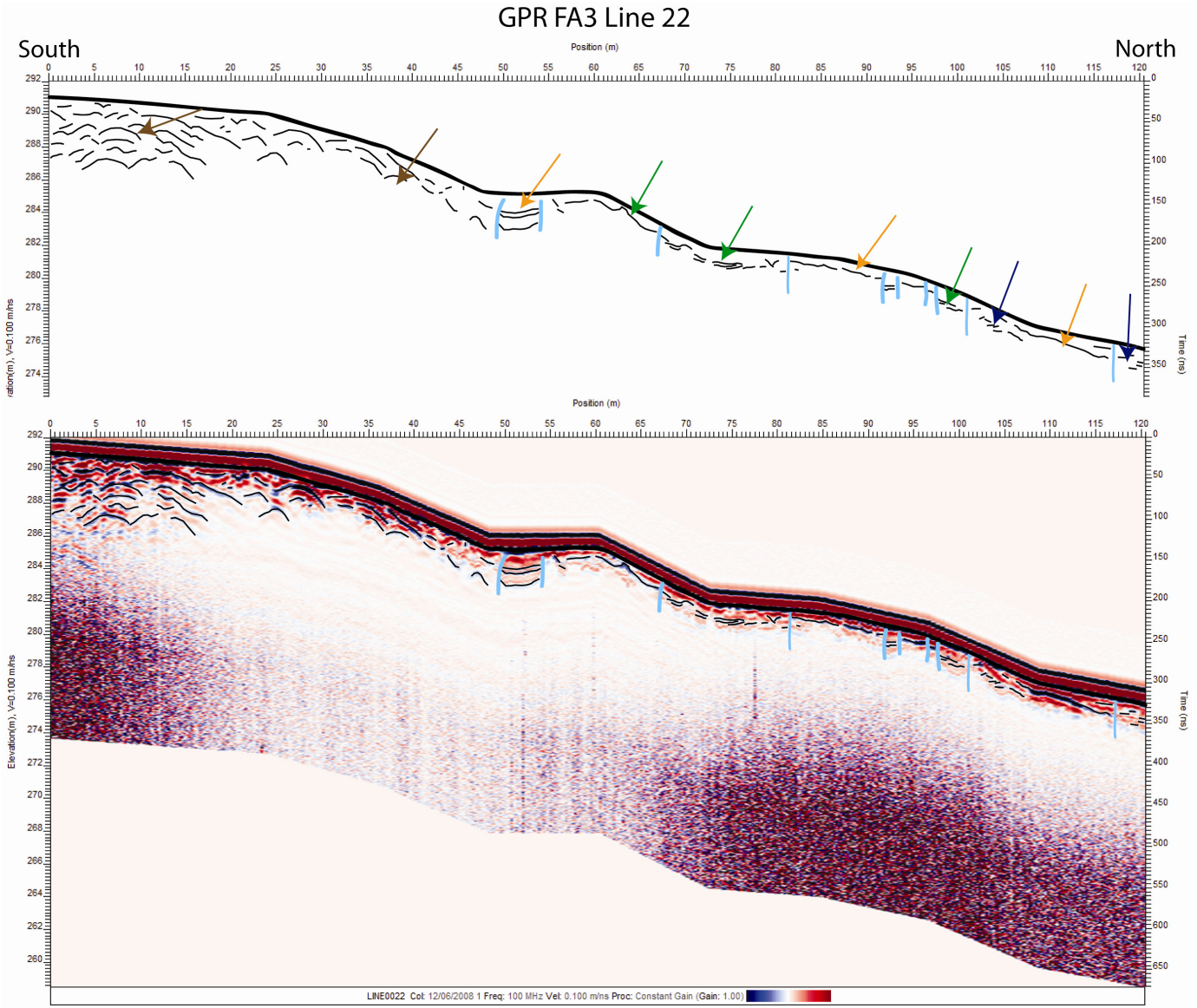

Figure 43. GPR transect within FA3: Line 22. Colored arrows correspond with GPR radar facies by Ekes and Friele (2003), as seen in Figure 37.

Chapter 4: Discussion

4.1 Fault Geometry and Geomorphology

The faults in all field areas juxtapose mid-Cretaceous Alisitos arc volcanic rocks or the arc-related intrusion with Quaternary alluvial deposits or cut entirely through Quaternary alluvium. The fault contacts are marked either by lithologic contacts that display topographic variation between the units or recognizable geomorphic features. The presence of dextrally offset stream channels, recent fault scarps and fault rocks along the fault zones of all three field areas indicate the location of the fault traces and, very importantly, also demonstrate recent activity along the main fault and fault splays. The number of fault splays expressed at the surface increases westward. Only one minor splay occurs in FA3, whereas a well-developed splay is found in FA2, and two extensive splays are present in FA1, demonstrating westward-increasing complexity within this fault system. The complexity of the fault system and the presence of different fault splays are not discussed by Schug (1987). In fact, Schug (1987) states that the fault system is represented by a single, near vertical fault trace "without significant branches or splays." Apparently he did not recognize the two significant southward steps along the mountain front and the geomorphic evidence along that part of Punta Banda ridge that suggest recent fault activity and greater complexity in the system.

Interestingly, the southernmost fault splays in FA1 and FA2 along the southward steps of the mountain front are marked by exceptionally well-developed triangular facets, which are more typical for dip-slip or oblique-slip faults (Bull, 2007). Furthermore, slickenlines on slickensided surfaces and on shear fractures in FA1 and FA2 are moderately plunging (Alsleben, personal communication, 2009), which is not expected in a strike-slip-dominated system, where one would expect subhorizontal or shallowly

plunging slickenlines. Overall, slickenlines indicate either northeast-side down, normal/dextral or northeast-side up, reverse/sinistral displacement along these faults. Although slickenlines cannot be used to properly determine relative motions, combining slickenline measurements with the existence of well-developed triangular facets and dextrally offset stream channels, supports oblique movement along the fault in a normal/dextral sense. No previous authors recognize a normal/dextral component along the Agua Blanca fault system, although Schug (1987) acknowledges conclusions by Gastil and Marshall (1980) that the San Miguel fault system displays a normal oblique component.

4.2 Bedrock Geology

The main bedrock units exposed in the study area are largely volcanic and volcaniclastic rocks related to the mid-Cretaceous Alisitos arc. Within the study area, these rocks largely consist of plagioclase-rich volcanic rocks that resemble the Alisitos arc volcanics described elsewhere (Allison, 1955; Suarez-Vidal, 1987). The small tonalite intrusion in FA2 is also typical for the suite of Cretaceous plutons that make up much of the Peninsular Ranges batholith in southern California and Baja California (e.g., Gastil *et al.*, 1975; Johnson *et al.*, 1999; Wetmore *et al.*, 2003).

Sandstones and conglomerates exposed in FA2 are the only rocks of the El Rosario Formation in the field area. These observations contradict conclusions by Schug (1987), who suggests that most ridges and scarps north of the main Agua Blanca fault are underlain by the El Rosario Formation. The contact between the El Rosario and Alisitos Formations is not exposed in most areas. However, elsewhere it is clearly demonstrated that the upper Cretaceous El Rosario Formation unconformably overlies

the mid-Cretaceous Alisitos arc volcanics (Suarez-Vidal, 1987), and limited observations presented here do not disagree with that conclusion.

4.3 Quaternary Alluvial Deposits

The Quaternary alluvial units are gravel alluvial fan deposits. These types of deposits are created when streams travel down high relief structures such as the escarpment of an active fault zone and lose channel confinement (Reading, 1996). The sediment spreads out onto a valley floor. Where sediment supply is high enough for several fans to occur contemporaneously, adjacent fan deposits can coalesce into a smooth ramp extending into the valley (Reading, 1996). Valle Maneadero is a coastal plain bounded by the escarpment (Punta Banda Ridge) of an active fault. The alluvial deposits collecting at the base of this escarpment have coalesced to form a smooth ramp that extends into the valley, except where the flow is blocked by shutter ridges. In these blocked areas, sediment is trapped behind these shutter ridges and accumulates until the obstruction is breached (Reading, 1996).

Classifications of the Quaternary alluvial packages by myself and Schug (1987) are based on different methodology; however, the conclusions are in agreement. Schug (1987) used aerial photographs (1:25,000 scale) enlarged to 1:5,000 scale for detailed geomorphic mapping to recognize seven distinct Quaternary alluvial units along the main fault trace. He completed a trenching study to classify alluvial packages based on variably-developed soil horizons and ^{14}C dating of charcoal layers and found evidence for the incorporation of Holocene sediments in offset layers, which demonstrates recent activity along the Agua Blanca fault. I mapped the study area on foot using a ~1:10,000 scale topographic base map, and classified the alluvial packages based on

geomorphology and topographic expression. Interpretations of geomorphic features, such as triangular facets, offset stream channels, fault scarps, pressure ridges and shutter ridges and a possible pressure ridge lead to the conclusion that the fault has recently been active.

4.4 Significance of GPR Sections

The GPR surveys were completed on gravel alluvial fan deposits. Ekes and Friele (2003) have used GPR surveys to identify radar facies that correspond with sedimentological facies within gravel alluvial fan deposits. The results by Ekes and Friele (2003) were used as a model for identification and interpretation of radar facies within the GPR sections of this study (Figure 37).

Ekes and Friele (2003) completed GPR surveys on the Cheekye Fan, a gravel alluvial fan in southwestern British Columbia, Canada. They identified ten facies packages, of which six correspond to facies identified in the gravel alluvial fans along the Agua Blanca fault (Figure 37). GPR sections are based on reflector continuity, shape and amplitude, configuration of reflections within the supposed bedforms, and external configuration of the bedforms with respect to each other. The laterally continuous reflectors in the GPR sections of my study correlate with radar facies 4, which is defined as horizontally bedded sheetflood gravels or clast-rich debris-flow deposits (Figure 37). The less continuous, sometimes wavy reflectors are equivalent to radar facies 3, interpreted as poorly bedded sheetflood gravels or matrix-rich debris-flow deposits. The chaotic, poorly defined reflectors, which correspond to radar facies number 5, are defined as matrix-rich debris-flow deposits. The convex reflectors correspond to radar facies 2, which suggests buried pipes, trees and other objects that

interfere with GPR signals. The concave reflectors represent radar facies 6, interpreted as possible buried stream channels. The parabolic interference forms agree with radar facies 1, which is classified as bedrock (Ekes and Friele, 2003).

The complexity of the fault system is subtle. Based on the GPR data, I suggest that a greater number of faults exists than are actually exposed at the surface. However, while disturbances in the reflectors were pervasive and offset several layers within the section, the disturbances were only slight. Therefore it is possible that not all disturbances that were identified as faults are in fact faults. The resolution and penetration of the GPR were not what was expected, even though we followed a similar method to that successfully used in other studies of fault systems (Cai *et al.*, 1996; Yetton and Nobes, 1998). This could be the result of several factors, such as scattering due to the medium through which the GPR sections were captured, the nearness of the water table to the surface within the field areas or the parameters set for the GPR surveys. Ekes and Friele (2003) used 50 MHz antennae to complete their surveys and they achieved markedly better penetration and resolution than our survey using 100 MHz antennae.

Chapter 5: Conclusions and Implications

5.1 Conclusions

As stated at the outset, the three main questions to be answered by the project are as follows. Is the Agua Blanca fault currently active? If the fault has recently been active, how is the fault expressed at the surface? What is the character of the fault in the subsurface?

The geomorphology along the western segment of the Agua Blanca fault suggests that the fault has recently been active. Geomorphic features, such as deflected stream channels and recent fault scarps, indicate recent movement along the fault system. The surface expression of the fault system is also characterized by fault breccia and gouge, triangular facets, and abrupt changes in topography. The interpretation that the fault has been recently active agrees with that of several previous authors (Schug, 1987; Rockwell *et al.*, 1993; Dixon *et al.*, 2002). The slickenlines on slickensided surfaces and the well-developed triangular facets also indicate the presence of a normal oblique component that has not been previously noted, in addition to the overall dextral motion of the Agua Blanca fault system.

The subsurface characteristics of the fault as determined by GPR indicate a more complex system than originally postulated by previous authors (Allen *et al*., 1960; Schug. 1987). The splays interpreted in my study disagree with the study by Schug (1987), which is the most recent geomorphic field work completed on the western segment of the Agua Blanca fault.

5.2 Implications for future studies

To substantiate the above results, additional studies of the fault system should be completed. Valle Santo Tomas to the east of the study area is a logical target for future study. Similar geomorphic mapping and GPR surveys are desirable and would allow correlation with the results presented here.

The fault traces in the GPR sections from this study are not highly pronounced. There are, however, several fault traces visible on the GPR sections that are not expressed at the surface. This complex pattern seems pervasive along the Punta Banda segment of the fault, but whether the fault zone is as complex to the east remains to be evaluated. Furthermore, the present study only utilized the 100 MHz antennae. Perhaps future studies can experiment with both the 50 MHz antennae and 100 MHz antennae, to determine the best possible compromise between depth of penetration and signal resolution for this region.

References Cited

Allen, C.R., L. Silver, and F.G. Stehli, 1960. Agua Blanca fault, a major transverse structure of northern Baja California, Mexico. Geological Society of America Bulletin, vol. 71, p. 457 - 482.

Allison, E.C., 1955. Middle Cretaceous gastropoda from Punta China, Baja California, Mexico. Journal of Paleontology, vol. 29, p. 400 - 432.

Atwater, T.M., 1970. Implications of plate tectonics for the Cenozoic tectonic evolution of western North America. Geological Society of America Bulletin, vol. 81, p. 3513 - 3536.

Atwater, T., 1989. Plate tectonic history of the northeast Pacific and western North America, *in* The geology of North America, Vol. N: The northeastern Pacific Ocean and Hawaii, edited by E.L. Winterer, D.M. Hussong and R.W. Decker. Geological Society of America, p. 21 - 72.

Atwater, T.M. and J. Stock, 1998. Pacific-North America plate tectonics of the Neogene southwestern United States: an update. International Geology Review, vol. 40, p. 375 - 402.

Baker, G.S., T.E. Jordan, and J. Pardy, 2007. An introduction to ground penetrating radar (GPR), *in* Stratigraphic analyses using GPR, edited by G.S. Baker and H.M. Jol. Geological Society of America Special Paper 432, p. 1 - 18.

Bose, E., and E. Wittich, 1913. Informe relativo a la exploracion de la region norte de la costa occidental de la Baja California. Geological Institute of Mexico, Parergones, vol. 4, p. 307 - 529.

Bull, W.B., 2007. Tectonic geomorphology of mountains, a new approach to paleoseismology. Blackwell Publishing, MA, p. 1 - 274.

Burger, H.R., A.F. Sheehan, and C.H. Jones, 2006. Introduction to Applied Geophysics: Exploring the Shallow Subsurface. W.W. Norton and Company, NY, NY, p. 499 - 554.

Cai, J., G.A McMechan, and M.A. Fisher, 1996. Application of ground-penetrating radar to investigation of near-surface fault properties in the San Francisco Bay region. Bulletin of the Seismological Society of America, vol. 86, p. 1459 - 1470.

Dickinson, W.R., and W.S. Snyder, 1979. Geometry of triple junctions related to San Andreas transform. Journal of Geophysics, vol. 84, p. 561 - 572.

Dickinson, W.R., 1996. Kinematics of transrotational tectonism in the California transverse ranges and its contribution to cumulative slip along the San Andreas transform fault system. Geological Society of America Special Paper 305, p. 1 - 46.

Dixon, T., J. Decaix, F. Farina, K. Furlong, R. Malservisi, R. Bennett, F. Suarez-Vidal, J. Fletcher, and J. Lee, 2002. Seismic cycle and rheological effects on estimation of present-day slip rates for the Agua Blanca and San Miguel-Vallecitos faults, northern Baja California, Mexico. Journal of Geophysical Research, vol. 107, p. 5 - 1 to 5 - 23.

Ekes, C., and P. Friele, 2003. Sedimentary architecture and post-glacial evolution of Cheekye fan, southwestern British Columbia, Canada *in*: Ground Penetrating Radar in Sediments, edited by C.S. Bristow and H.M. Jol. Geological Society of London Special Publication 211, p. 87 - 98.

Fackler-Adams, B.N. and C.J. Busby, 1998. Structural and stratigraphic evolution of extensional oceanic arcs. Geology, vol. 26, p. 735 - 738.

Floras, T., 1931, Carta geologica de la Baja California: Cartas Geol. y Min. de la Rep. Mexicana, p. 1 - 22.

Gastil, R.G., R.P. Phillips, and E.C. Allison, 1975. Reconnaissance geology of the state of Baja California: GSA Memoir 140. p. 170

Gastil, R.G., and M. Marshall, 1980. The San Miguel fault zone, Baja California, Mexico: Summaries of Technical Reports. Volume X, National Earthquake Hazards Reduction Program, United States Geological Survey, Open File Report 80-842.

Gastil, R.G., G.J. Morgan, and D. Krummenacher, 1981. Tectonic History of Peninsular California and Adjacent Mexico *in* Rubey Volume No.1, The Tectonic Development of California, edited by G. Ernst, Freeman Press, p.284 - 306.

Hatch, M., 1987. Neotectonics of the Agua Blanca fault, Valle Agua Blanca, Baja California, Mexico. Master's Thesis, San Diego State University.

Hatcher, R.D., 1995. Structural Geology – Principles, concepts, and problems. Prentice-Hall, Inc. Second edition, p. 245

Hilinski, T., 1988. Structure and Quaternary faulting about the eastern terminus of the Agua Blanca fault, Baja California, Mexico. Master's Thesis, San Diego State University.

Irwin, W.P., 1990. Geology and plate-tectonic development *in* The San Andreas fault system, California, edited by R.E. Wallace. U.S. Geological Survey Professional Paper 1515. p. 61 - 77.

Johnson, S.E., M.C. Tate, C.M. Fanning, 1999. New geologic mapping and SHRIMP U-Pb zircon data in the Peninsular Ranges batholith, Baja California, Mexico: Evidence for a suture?. Geology, vol. 27, p. 743 - 746.

Kimbrough, D.L., D.P. Smith, J.B. Mahoney, T.E. Moore, M. Grove, R.G. Gastil and A. Ortega-Rivera, 2001. Forearc-basin sedimentary response to rapid late Cretaceous

batholith emplacement in the Peninsular Ranges of southern and Baja California. Geology, vol. 29, p. 491 - 494.

Legg, M.R., V. Wong O., F. Suarez-Vidal, 1991. Geological structure and tectonics of the Inner Continental Borderland of northern Baja California *in* Gulf and peninsular province of the Californias, edited by J. Dauphin and B. Simoneit, AAPG Memoir 47, p.145 - 177

Lescinsky, H.L.,J. Ledesma-Vazquez, M.E. Johnson, 1991. Dynamics of Late Cretaceous rocky shores (Rosario formation) from Baja California, Mexico. PALAIOS, vol. 6, p. 126 - 141.

McKenzie, D.P., and W.J. Morgan, 1969. Evolution of triple junctions. Nature, vol. 224, p. 125 - 133.

Reading, H.G., 1996. Sedimentary Environments: Processes, Facies and Stratigraphy. Third edition, p. 57 - 65.

Rockwell, T.K., D.L. Schug, and M.E. Hatch, 1993. Late Quaternary slip rates along the Agua Blanca fault, Baja California, Mexico: *in* Geological investigations of Baja California, edited by P.L. Abbott. South coast geological society annual field trip guidebook, p. 53 - 92.

Santillan M., and T. Barrera, 1930. Las posibilidades petrollferas en la costa occidental de la Baja California, *in* los paralelos 30° y 32° de latitud norte: Anales del Institute Geologia (Mexico), vol. 5, p. 1 - 37.

Schug, D.L., 1987. Neotectonics of the western reach of the Agua Blanca fault Baja California, Mexico. Master's Thesis, San Diego State University.

Slater, L. and T. Niemi, 2003. Ground-penetrating radar investigation of active faults along the Dead Sea transform and implications for seismic hazards within the city of Aqaba, Jordan. Tectonophysics, vol. 368, p. 33 - 50.

Stock, J. and P. Molnar, 1988. Uncertainties and implications of the late Cretaceous and Tertiary position of North America relative to the Farallon, Kula, and Pacific plates. Tectonics, vol. 7, p. 1339 - 1384.

Suarez-Vidal, F., 1987. The calcareous facies of the Alisitos formation, evidence for an Early Cretaceous tectonic calm. Ciencias Marinas, vol. 13, p. 131 - 154.

Suarez-Vidal, R., G. Armijo, P. Morgan, R. Bodon, and G. Gastil, 1991. Framework of recent and active faulting in northern Baja California *in* Gulf and peninsular province of the Californias, edited by J. Dauphin and B. Simoneit. AAPG Memoir 47, p. 285 - 300.

Thatcher, W., 1990. Present-day crustal movements and the mechanics of cyclic deformation *in* The San Andreas fault system, California, edited by R.E. Wallace. U.S. Geological Survey Professional Paper 1515, p. 189 - 203.

Wallace, R.E., 1990. The San Andreas Fault System, California. U.S. Geological Survey Professional Paper 1515, p. 1 - 283.

Wesnousky, S., 2005. The San Andreas and Walker Lane fault systems, western North America: transpression, transtension, cumulative slip and the structural evolution of a major transform plate boundary. Journal of Structural Geology, vol. 27, p. 1505 - 1512.

Wetmore, P.H., K.L. Schmidt, S.R. Paterson, C. Herzig, 2002. Tectonic implications for the along-strike variation of the Peninsular ranges batholith, southern and Baja California. Geology, vol. 30, p. 247 - 250.

Wetmore, P.H., C. Herzig, H. Alsleben, M. Sutherland, K.L. Schmidt, P.W. Schultz, and S.R. Paterson, 2003. Mesozoic tectonic evolution of the Peninsular Ranges of southern and Baja California, *in* Tectonic evolution of northwestern Mexico and the southwestern USA, edited by S.E. Johnson, S.R. Paterson, J.M. Fletcher, G.H. Girty, D.L. Kimbrough, and A. Martin-Barajas. Geological Society of America Special Paper 374, p. 93 - 116.

Wilson, D.S., 1988. Tectonic history of the Juan de Fuca ridge over the last 40 million years. Journal of Geophysics, vol. 93, p. 11863 - 11876.

Woodford, A. O., and T.F. Harris, 1938. Geological reconnaissance across Sierra San Pedro Martir, Baja California. Geological Society of America Bulletin, vol. 49, p. 1297 - 1336.

Yetton, M.D., and D.C. Nobes, 1998. Recent vertical offset and near-surface structure of the Alpine fault in Westland, New Zealand, from ground penetrating radar profiling. New Zealand Journal of Geology and Geophysics, vol. 41, p. 485 - 492.

Vita

Personal	Sarah Ruth Madsen
Background	Fort Worth, Texas
Born	November 10, 1982, San Antonio, TX
Parents	Randy and Cindi Haben
Married	Nathan Madsen July 16, 2005
Education	Bachelor of Science in Geosciences December 2006
Experience	Intern Geologist Summer 2004 – Winter 2006 Matador Resources Dallas, TX
	Intern Geologist Spring 2007 Hess Corporation Houston, TX
	Intern Geologist Summer 2007 EnCana Oil and Gas Inc. Dallas, TX
	Intern Geologist Summer 2009 Pioneer Natural Resources Inc. Denver, CO

Abstract

GEOMORPHIC MAPPING AND GROUND-PENETRATING RADAR SURVEY OF THE WESTERN SEGMENT OF THE AGUA BLANCA FAULT, BAJA CALIFORNIA, MEXICO

By Sarah Ruth Madsen, M.S., 2009
Department of Geology
Texas Christian University

Dr. Helge Alsleben – Assistant Professor of Geology

The Agua Blanca fault system is a dextral strike-slip fault system in northwestern Baja California, Mexico. Despite no historic seismic activity, the geomorphology suggests that the fault is active. Geomorphic maps (~1:10,000) were completed within three field areas along the western segment of the main fault. Diagnostic features such as deflected stream channels provide evidence of recent fault activity. The presence of well-developed triangular facets suggests an additional normal component to this strike-slip system. Ground-penetrating radar surveys were conducted to image the fault in the near surface. Many more fault splays were mapped within the sections than were visible at the surface, indicating the complexity of the fault system. Alluvial surfaces were identified within the sections and characterized based on continuity and shape of reflectors.